2. Berger EA, Doms RW, Fenyo EM, Korber BT, Littman DR, Moore JP, et al. A new classification for HIV-1. Nature. 1998;391(6664):240.
3. Moore JP, Kitchen SG, Pugach P, Zack JA. The CCR5 and CXCR4 coreceptors – central to understanding the transmission and pathogenesis of human immunodeficiency virus type 1 infection. AIDS Res Hum Retroviruses. 2004;20(1):111–26.
4. Iwamoto A, Hosoya N, Kawana-Tachikawa A. HIV-1 tropism. Protein Cell. 2010;1(6):510–3.
5. Fatkenheuer G, Nelson M, Lazzarin A, Konourina I, Hoepelman AI, Lampiris H, et al. Subgroup analyses of maraviroc in previously treated R5 HIV-1 infection. N Engl J Med. 2008;359(14):1442–55.
6. Saag M, Goodrich J, Fatkenheuer G, Clotet B, Clumeck N, Sullivan J, et al. A double-blind, placebo-controlled trial of maraviroc in treatment-experienced patients infected with non-R5 HIV-1. J Infect Dis. 2009;199(11):1638–47.
7. Shioda T, Levy JA, Cheng-Mayer C. Macrophage and T cell-line tropisms of HIV-1 are determined by specific regions of the envelope gp120 gene. Nature. 1991;349(6305):167–9.
8. Hwang SS, Boyle TJ, Lyerly HK, Cullen BR. Identification of the envelope V3 loop as the primary determinant of cell tropism in HIV-1. Science. 1991;253(5015):71–4.
9. Cocchi F, DeVico AL, Garzino-Demo A, Cara A, Gallo RC, Lusso P. The V3 domain of the HIV-1 gp120 envelope glycoprotein is critical for chemokine-mediated blockade of infection. Nat Med. 1996;2(11):1244–7.
10. Hoffman TL, Doms RW. HIV-1 envelope determinants for cell tropism and chemokine receptor use. Mol Membr Biol. 1999;16(1):57–65.
11. Harrigan PR, Geretti AM. Genotypic tropism testing: evidence-based or leap of faith? AIDS. 2011;25(2):257–64.
12. Vandekerckhove LP, Wensing AM, Kaiser R, Brun-Vezinet F, Clotet B, De Luca A, et al. European guidelines on the clinical management of HIV-1 tropism testing. Lancet Infect Dis. 2011;11(5):394–407.
13. Whitcomb JM, Huang W, Fransen S, Limoli K, Toma J, Wrin T, et al. Development and characterization of a novel single-cycle recombinant-virus assay to determine human immunodeficiency virus type 1 coreceptor tropism. Antimicrob Agents Chemother. 2007;51(2):566–75.
14. Wang J, Kondo N, Long Y, Iwamoto A, Matsuda Z. Monitoring of HIV-1 envelope-mediated membrane fusion using modified split green fluorescent proteins. J Virol Methods. 2009;161(2):216–22.
15. Kondo N, Miyauchi K, Meng F, Iwamoto A, Matsuda Z. Conformational changes of the HIV-1 envelope protein during membrane fusion are inhibited by the replacement of its membrane-spanning domain. J Biol Chem. 2010;285(19):14681–8.
16. Soda Y, Shimizu N, Jinno A, Liu HY, Kanbe K, Kitamura T, et al. Establishment of a new system for determination of coreceptor usages of HIV based on the human glioma NP-2 cell line. Biochem Biophys Res Commun. 1999;258(2):313–21.
17. Shimizu N, Tanaka A, Oue A, Mori T, Ohtsuki T, Apichartpiyakul C, et al. Broad usage spectrum of G protein-coupled receptors as coreceptors by primary isolates of HIV. AIDS. 2009;23(7):761–9.
18. Murray EJ, Leaman DP, Pawa N, Perkins H, Pickford C, Perros M, et al. A low-molecular-weight entry inhibitor of both CCR5- and CXCR4-tropic strains of human immunodeficiency virus type 1 targets a novel site on gp41. J Virol. 2010;84(14):7288–99.
19. Kramer VG, Schader SM, Oliveira M, Colby-Germinario SP, Donahue DA, Singhroy DN, et al. Maraviroc and other HIV-1 entry inhibitors exhibit a class-specific redistribution effect that results in increased extracellular viral load. Antimicrob Agents Chemother. 2012;56(8):4154–60.
20. Chang CH, Hinkula J, Loo M, Falkeborn T, Li R, Cardillo TM, et al. A novel class of anti-HIV agents with multiple copies of enfuvirtide enhances inhibition of viral replication and cellular transmission in vitro. PloS One. 2012;7(7):e41235.
21. Vila-Coro AJ, Mellado M, Martin de Ana A, Lucas P, del Real G, Martinez AC, et al. HIV-1 infection through the CCR5 receptor is blocked by receptor dimerization. Proc Natl Acad Sci U S A. 2000;97(7):3388–93.
22. Badr G, Borhis G, Treton D, Moog C, Garraud O, Richard Y. HIV type 1 glycoprotein 120 inhibits human B cell chemotaxis to CXC chemokine ligand (CXCL) 12, CC chemokine ligand (CCL)20, and CCL21. J Immunol. 2005;175(1):302–10.
23. Lin NH, Negusse DM, Beroukhim R, Giguel F, Lockman S, Essex M, et al. The design and validation of a novel phenotypic assay to determine HIV-1 coreceptor usage of clinical isolates. J Virol Methods. 2010;169(1):39–46.
24. Zhu P, Liu J, Bess J, Jr., Chertova E, Lifson JD, Grise H, et al. Distribution and three-dimensional structure of AIDS virus envelope spikes. Nature. 2006;441(7095):847–52.
25. Reeves JD, Coakley E, Petropoulos CJ, Whitcomb JM. Coreceptor tropism assay for selecting patients for therapy with entry inhibitors targeting CCR5: a review of analytical and clinical studies. J Viral Entry. 2009;3(3):94–102.

SCIENTIFIC REPORTS

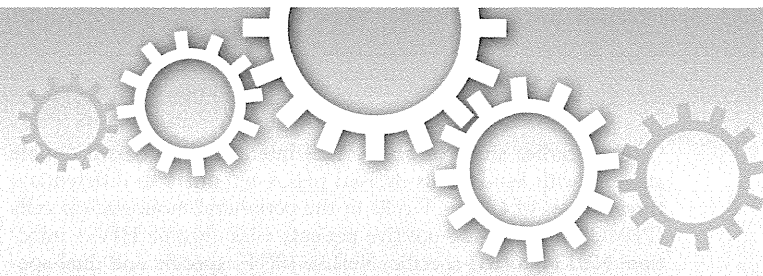

OPEN

SUBJECT AREAS:
VIRAL HOST RESPONSE
HIV INFECTIONS
ADAPTIVE IMMUNITY

Received
15 July 2013

Accepted
15 October 2013

Published
6 November 2013

Correspondence and requests for materials should be addressed to A.I. (aikichi@ra3.so-net.ne.jp; aikichi@ims.u-tokyo.ac.jp)

# Structure of TCR and antigen complexes at an immunodominant CTL epitope in HIV-1 infection

Akihisa Shimizu[1], Ai Kawana-Tachikawa[1], Atsushi Yamagata[2,3], Chungyong Han[1], Dayong Zhu[4], Yusuke Sato[2,3], Hitomi Nakamura[4,5], Tomohiko Koibuchi[5], Jonathan Carlson[6], Eric Martin[7], Chanson J. Brumme[8], Yi Shi[9], George F. Gao[9], Zabrina L. Brumme[7,8], Shuya Fukai[2,3,10] & Aikichi Iwamoto[1,4,5]

[1]Division of Infectious Diseases, Advanced Clinical Research Center, the Institute of Medical Science, the University of Tokyo. 4-6-1 Shirokanedai, Minato-ku, Tokyo 108-8639, Japan, [2]Structural Biology Laboratory, Life Science Division, Synchrotron Radiation Research Organization and Institute of Molecular and Cellular Biosciences, the University of Tokyo. 1-1-1, Yayoi, Bunkyo-ku, Tokyo 113-0032, Japan, [3]Department of Medical Genome Sciences, Graduate School of Frontier Sciences, The University of Tokyo. 5-1-5 Kashiwanoha, Kashiwa-shi, Chiba 277-8561, Japan, [4]Department of Infectious Disease Control, the International Research Center for Infectious Diseases, the Institute of Medical Science, the University of Tokyo. 4-6-1 Shirokanedai, Minato-ku, Tokyo 108-8639, Japan, [5]Department of Infectious Diseases and Applied Immunology, Hospital, the Institute of Medical Science, the University of Tokyo. 4-6-1 Shirokanedai, Minato-ku, Tokyo 108-8639, Japan, [6]Microsoft Research, Los Angeles, CA, USA. 1100 Glendon Ave PH-1. Los Angeles, CA 90024, USA, [7]Faculty of Health Sciences, Simon Fraser University. 8888 University Drive, Burnaby, BC, Canada V5A 1S6, [8]British Columbia Centre for Excellence in HIV/AIDS. 608–1081 Burrard Street, Vancouver, BC, Canada V6Z 1Y6, [9]CAS Key Laboratory of Pathogenic Microbiology and Immunology, Institute of Microbiology, Chinese Academy of Sciences. No. A3 Datun Road, Chaoyang District, Beijing 100101, China, [10]JST, CREST, 1-1-1, Yayoi, Bunkyo-ku, Tokyo 113-0032, Japan.

**We investigated the crystal structure of an HLA-A*2402-restricted CTL epitope in the HIV-1 *nef* gene (Nef134-10) before (pHLA) or after TCR docking. The wild type epitope and two escape mutants were included in the study. Y135F was an early-appearing major mutation, while F139L was a late-appearing mutation which was selected in the patients without Y135F. F139 was an eminent feature of the Nef134-10 epitope. Wild type-specific TCR was less fit to F139L mutant suggesting that F139L is an escape from the CTL against the wild type epitope. Although Y135F mutation disrupted the hydrogen bond to HLA-A*2402 His70, newly formed hydrogen bond between T138 and His70 kept the conformation of the epitope in the reconstituted pMHC. TCR from Y135F- or dually-specific CTL had unique mode of binding to the mutant epitope. Y135F has been reported as a processing mutant but CTL carrying structurally adequate TCR can be found in the patients.**

Cytotoxic T lymphocytes (CTL) can exert an efficient control on HIV-1 replication if HIV-1 antigens are presented on the surface of infected cells and properly recognized by the heterodimeric T cell receptors (TCR) attached to the CTL[1–4]. For this to occur, viral proteins synthesized in the infected cells must first be digested to fragments, transported to the rough endoplasmic reticulum (ER), and bound within a groove formed by two α-helices of the major histocompatibility complex (HLA in human) class I molecules as a 8–10-mer peptide[5–7]. The peptide-bound HLA class I molecules (pHLA) are then exported to the cell surface for recognition by TCR on the CTL cell membranes[8,9]. The encounter between TCR and pHLA is the fundamental requirement and initial step that allows CTL to deliver their cytotoxicity.

The genetic hypermutability of HIV-1 can interfere with immune surveillance by CTL by introducing amino acid changes that allow the virus to "escape" immune recognition. Escape phenomena may occur at different steps during the process of antigen presentation and recognition. Mutations can result in changes in processing the viral proteins or in the way such that the processed peptides cannot bind to the HLA molecules or the pHLA cannot interact properly with TCR. For example, a CTL epitope in the HIV-1 *nef* gene, Nef134-10 (RYPLTFGWCF), is highly immunogenic in HLA-A*2402 (HLA-A24)-positive patients[10,11]. At a very early phase of primary HIV-1 infection, a Tyr-to-Phe mutation at the 2nd position of the Nef134-10 epitope (Y135F; Nef134-10(2F)) is frequently selected. HLA-A24 is the most prevalent HLA class I allele among Japanese[12].

In an earlier study of pHLA/TCR interactions, we used double staining with Sendaivirus-derived pHLA-tetramers to differentiate three classes of CD8+ T cells in the peripheral mononuclear cells (PBMC) of HLA-A24-positive patients with chronic HIV-1 infection: Nef134-10(wt)-specific, Nef134-10(2F)-specific and dual-specific (reacting to both wt and 2F epitopes)[13,14]. Since the encounter between TCR and pHLA is critical for CTL activation, structural studies examining the interactions between pHLA and TCR should be highly relevant in understanding the immune response to HIV-1 infection, including viral escape from immune surveillance. However, very few crystal structures relevant to escape mutations have been solved to date. To gain insights into the battle between HIV-1 and cellular immune responses we established CTL clones representing each of the three classes of antigen specificity targeting the Nef134-10 epitope, reconstituted the pHLA/TCR interactions *in vitro*, and solved the crystal structures. In the small number of patients without Y135F mutation, F139L mutation was selected. Since a wild type specific TCR showed a substantial affinity to the epitope with F139L mutation (Nef134-10(6L)), we also solved the crystal structure of the pHLA/TCR interaction between them.

## Results

**Characterization of escape mutations and specific T cell responses by chromium release and sequencing.** Before initiating studies on the interactions between the epitope and T cell receptors, we examined the prevalence of HLA-A24-related mutations in the Nef134-10 epitope in two independent HIV-1 cohorts: the IMSUT cohort (188 Japanese HIV-1-positive individuals in Tokyo) and the HOMER cohort (1018 HIV-1-positive individuals in British Columbia, Asian prevalence of 5%). The results confirmed the association between HLA-A24 and the Y135F mutation (Supplementary Fig. 1a, b). In both cohorts Y135F and F139L mutations were each significantly associated with the presence of HLA-A24 ($p < 0.0001$ and $p = 0.0017$, respectively). In a multicenter longitudinal acute/early infection cohort of 16 individuals expressing HLA-A24, we reconfirmed the previous finding that Y135F is selected very early after the estimated date of infection, while F139L appeared late ($p = 0.0046$) (Supplementary Fig. 1c).

Next we established cellular clones representing dual-specific, Nef134-10(wt)-specific, Nef134-10(2F)-specific CTL from HLA-A24-positive patients in the IMSUT cohort. We showed previously that TCR repertoire of the dual-specific CD8+ T cells was highly restricted[14]. TRBV4-1 and TRAV8-3 gene segments were used almost exclusively as TCR β and α chains, respectively. C1-28, which used TRBV4-1 and TRAV8-3 was established and analyzed further as a CTL clone representing the dual-specific population. The TCR repertoire of the wild type specific CD8+ T cells was more diverse than the dual-specific population, but TRBV7-9 was used in more than 25% of the population. CTL clone H27-14 which used TRBV7-9 was established and represented the wild type-specific population in this study. Nef134-10(2F)-specific CD8+ T cell population was rare even after ex vivo stimulation with the cognate peptide, however, we could establish CTL clone T36-5 which represented Nef134-10(2F)-specific population. Specificities of the clones were examined by conventional chromium release assay (Fig. 1a–c).

**Binding characteristics of purified TCR and pHLA.** The heavy chain and β2-microglobulin were expressed in *E. coli* and synthesized cognate peptides were refolded and pHLA was purified as previously described[15]. TCR derived from each CTL clone were cloned, expressed and purified from inclusion bodies of *E. coli*[16]. Refolded TCR and pHLA complexes were subjected to the surface plasmon resonance (SPR) assay (Biacore™).

Binding affinities observed between the pHLAs and TCRs are consistent with the results of the cellular killing assay (Table S3 and Supplementary Fig. 2), with the dissociation constant (KD) of the H27-14 TCR/pHLA complex increasing in the following order: A24/Nef134-10(wt) < A24/Nef134-10(6L) < A24/Nef134-10(2F). Functional TCRs against cognate epitopes have an estimated affinity ranging from 1–100 μM[17]. A CTL population with H27-14 TCR could recognize HIV-1-infected cells expressing the wild type A24/Nef134-10 epitope very well and could also recognize cells expressing A24/Nef134-10(6L), although less efficiently. However, H27-14 TCR affinity was too low to recognize A24/Nef134-10(2F). T36-5 TCR was highly specific against A24/Nef134-10(2F) but the TCR could recognize also with A24/Nef134-10(wt). C1-28 TCR bound almost equally with Nef134-10(wt) and Nef134-10(2F).

Kinetic analysis of H27-14 and T36-5 TCR with cognate epitopes (Table S3) yielded results that were compatible with results from equilibrium analysis. We were unable to perform kinetic analysis on C1-28 TCR due to low refolding yields.

**General structures of free pHLA and TCR-pHLA.** To reveal the structural differences posed by amino acid substitutions in the epitope, we determined and compared structures of A24/Nef134-10(wt), A24/Nef134-10(2F) and A24/Nef134-10(6L) before ligation to TCR (Fig. 2 and Supplementary Fig. 3a–c). The electron densities for three peptides that bound to HLA-A24 were unambiguous (Supplementary Fig. 4a–c). Large conformational changes were not seen when the Nef134-10(2F) and Nef134-10(6L) peptides in the groove of HLA-A24 were superimposed onto Nef134-10(wt) (Fig. 2a). Root mean square deviation (RMSD) values were 0.260Å

a

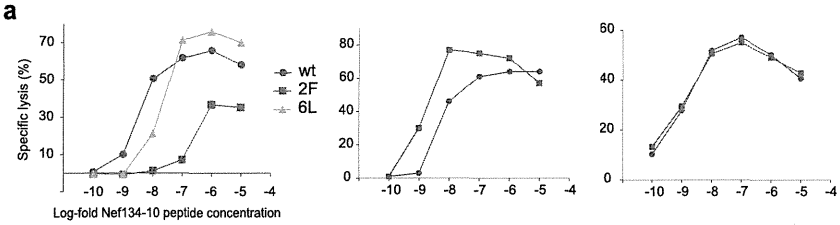


b

| TCR | H27-14 | T36-5 | C1-28 |
|---|---|---|---|
| Vα | 21 | 12-2 | 8-3 |
| CDR3α | AVRMDSSYKLIF | GTYNQGGKLI | AVGAPSGAGSYQLT |
| Vβ | 7-9 | 27 | 4-1 |
| CDR3β | ASSSWDTGELF | ASSGASHEQY | ASSPTSGIYEQY |

**Figure 1 | Specificities and TCR usage of the CTL clones specific to Nef134-10 epitopes.** (a) Cytolytic activities of HLA-A24-restricted Nef134-10-specific CTL clones derived from HLA-A24-positive HIV-1-infected patients. Clones H27-14 (left), T36-5 (middle) and C1-28 (right) killed HLA-A24-positive target cells pulsed with log-fold dilutions of Nef134-10 peptides, Nef134-10(wt); blue, Nef134-10(2F); red, Nef134-10(6L); orange. The effector-versus-target ratio was 5 : 1. (b) Vα and Vβ gene segments and CDR3 sequences of each CTL clone.

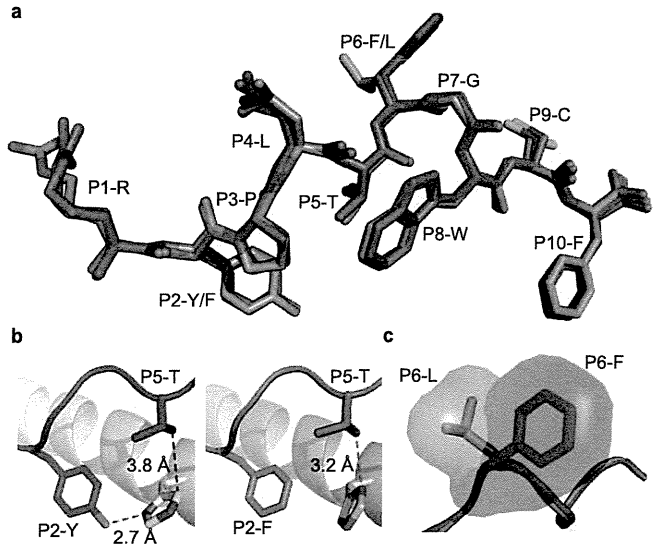


**Figure 2 | Conformation of the three Nef134-10 peptides in the complex with HLA-A24.** (a) Overlay of three Nef134-10 peptides (Nef134-10(wt), Nef134-10(2F) and Nef134-10(6L)) bound to the HLA-A24. Nef134-10(wt), Nef134-10(2F) and Nef134-10(6L) peptides are shown blue, red and orange stick representations, respectively. HLA-A24 binding groove are not shown for clarity. (b) Interaction between the Nef134-10 peptide and HLA-A24. P2-Tyr in the Nef134-10(wt) forms a hydrogen bond with His at position 70 in the HLA-A24 (**left**), while P5-Thr in the Nef134-10(2F) peptide forms a hydrogen bond with His70 (**right**). Red dashed lines indicate hydrogen bonds. A black dashed line indicates the shortest distance between P5-Thr in the Nef134-10(wt) and His70 in the HLA-A24. (c) The side chains of P6 in the Nef134-10(wt) and Nef134-10(6L) peptides, which protrude out of the HLA-A24 binding cleft, are shown as stick and surface representations. Nef134-10(wt) (blue) and Nef134-10(6L) (orange).

and 0.259Å, respectively. Y135(P2-Y) of the Nef134-10 (wt) peptide formed a hydrogen bond with His at position 70 of the HLA-A24 (His70), and T138(P5-T) of the Nef134-10(2F) peptide formed a potential hydrogen bond with His70 (Fig. 2b).

Side chains of L137(P4-L) and F139(P6-F) protruded from the A24 binding groove in the A24/Nef134-10, which appeared to be the eminent feature of this epitope. The solvent-accessible surface area of the side chain of Phe(F) of the Nef134-10(wt) epitope is larger than that of Leu(L) of the Nef134-10(6L) epitope by approximately 40Å$^2$ (188.2Å$^2$ for P6-F, 151.9Å$^2$ for P6-L) (Fig. 2c).

To understand how three TCRs (H27-14, T36-5 and C1-28) interact with their cognate pHLAs, we determined four TCR/pHLA complexes, including the H27-14 complexed to the agonist ligand, A24/Nef134-10(6L) (Supplementary Fig. 3d–g). The electron densities for CDR3 loops and peptide at the individual TCR/pHLA complex interfaces were unambiguous (Supplementary Fig. 4d–g).

Wild type-specific H27-14 TCR interacted with Nef134-10(wt), surrounding the F139(P6-F) residue by CDR loops (Fig. 3a, d). This complex exhibited a shape complementarity (Sc) of 0.75, which is at the higher end of the range of published TCR/pMHC[17]. R93α, Y98α and R31β of the H27-14 CDR rearranged to accommodate the aromatic residue of F139(P6-F) upon ligation, compared to their unligated state (Supplementary Fig. 5a, b). Y98α and R31β formed hydrogen bonds with T138(P5-T) (Supplementary Fig. 5b and Supplementary Table 3). The side chain of R93α rotated approximately 90° and formed a hydrogen bond with G100β, helping to stabilize CDRα and CDRβ at the TCR/pHLA interface.

In the T36-5-A24/Nef134-10(2F) complex, the A96 residue of CDR3β formed a hydrogen bond with the W141(P8-W) residue of Nef134-10(2F) upon ligation (Fig. 3b). The T36-5 TCR interacted with A24/Nef134-10(2F) over a wide range, with a BSA approximately 200 Å$^2$ higher than that of the other two complexes solved in this study (Fig. 3e and Supplementary Table 4) and with the highest affinity of the three TCRs in this study. The side chains of Y92α and H98β of the T36-5 TCR were packed against each other in the unligated state, but interacted with Nef134-10(2F) upon ligation (Supplementary Fig. 5c). Upon ligation the side chain of Q94α of the CDR3 loops moved 3.7 Å toward HLA-A24-α1 helix and contacted with the 135F(P2-F) carbonyl via a water molecule, while CDRβ loops (E30, A96 and H98) formed five hydrogen bonds with the amino acids (F6, G7, W8 and C9) located at the C-terminus of Nef134-10(2F) peptide.

In the C1-28-A24/Nef134-10(2F) complex, the CDR1α and 3β loops were located mainly above the Nef134-10(2F) peptide (Fig. 3c), whereas the CDR3α and 3β loops were located above the peptide in both H27-14-TCR-A24/Nef134-10(wt) and T36-5-TCR-A24/Nef134-10(2F) complexes (Fig. 3a, b). The side chains of Y32α and Y102α and the CDR3β loop surrounded the F139(P6-F) residue of the Nef134-10(2F) peptide. Water molecules acted as a "molecular glue" to stabilize the interface of the C1-28 TCR-A24/Nef134-10(2F) complex, but with only two hydrogen bonds between TCR and peptide in the C1-28-A24/Nef134-10(2F) complex, compared with four hydrogen bonds in the H27-14-A24/Nef134-10(wt) complex and five hydrogen bonds in the T36-5-A24/Nef134-10(2F) complex (Supplementary Table 3).

G28α and G98β formed hydrogen bonds with the side chains of the R134(P1-R) and C142(P9-C) residues, respectively. Surprisingly, the Vα domains, compared to Vβ domains, contributed more (~80%) in the interaction with A24/Nef134-10(2F) and were critical in the recognition of primarily the N-terminal part of the A24/Nef134-10(2F) by C1-28 TCR (Fig. 3c, f).

**Wild type-specific TCR against late/minor mutant.** H27-14 was slightly weaker in recognizing A24/Nef134-10(6L) than in recognizing A24/Nef134-10(wt) (Fig. 1a and Table S3). To evaluate the differences in binding ability to A24/Nef134-10(wt) or A24/Nef134-10(6L), we compared the structures of H27-14-A24/Nef134-10(wt) and H27-14-A24/Nef134-10(6L) (Fig. 4a). Conformational differences were minimal, with RMSDs of 0.485Å, 0.123Å and 0.109Å for the TCRs, Nef134-10 peptides and A24 binding clefts, respectively.

In H27-14-A24/Nef134-10(wt), the aromatic side chain of F139 (P6-F) protruding out of HLA-A24 binding groove was accommodated by the TCR pocket formed by the CDR1 and CDR3 loops, especially with Y31α, R93α, Y98α, R31β (Fig. 4b). Interestingly, the same binding mode was found in H27-14 TCR-A24/Nef134-10(6L) (Fig. 4c). The side chain of F139(P6-F) in the Nef134-10(wt) peptide was bulky. The 139L(P6-L) side chain in Nef134-10(6L) was much smaller, resulting in a gap in the TCR pocket surrounding the 139L(P6-L) side chain in the H27-14 TCR-A24/Nef134-10(6L) complex.

The number of van der Waals contacts (<4Å) between the TCR and P6 were 27 and 13 in H27-14-A24/Nef134-10(wt) and H27-14-A24/Nef134-10(6L), respectively. Additionally, cation-pi interactions between R93α or R31β and F139(P6-F) in H27-14-A24/Nef134-10(wt) were deformed in the case of 139L(P6L). The H27-14 TCR pocket surrounding P6 was a better fit for F139(P6-F) than for 139L(P6-L). This subtle structural difference might have been reflected in the killing assay and SPR (Fig. 1a and Table S3). Taken together, these results suggested that F139L mutation could be selected weakly but substantially as a minor escape mutant under the CTL pressure against the Nef134-10 epitope.

We were able to confirm the transformation from F to L at 6th position of Nef134-10 epitope in an HLA-A24-positive patient (Supplementary Fig. 6a). F139L appeared between Days 306 to 735

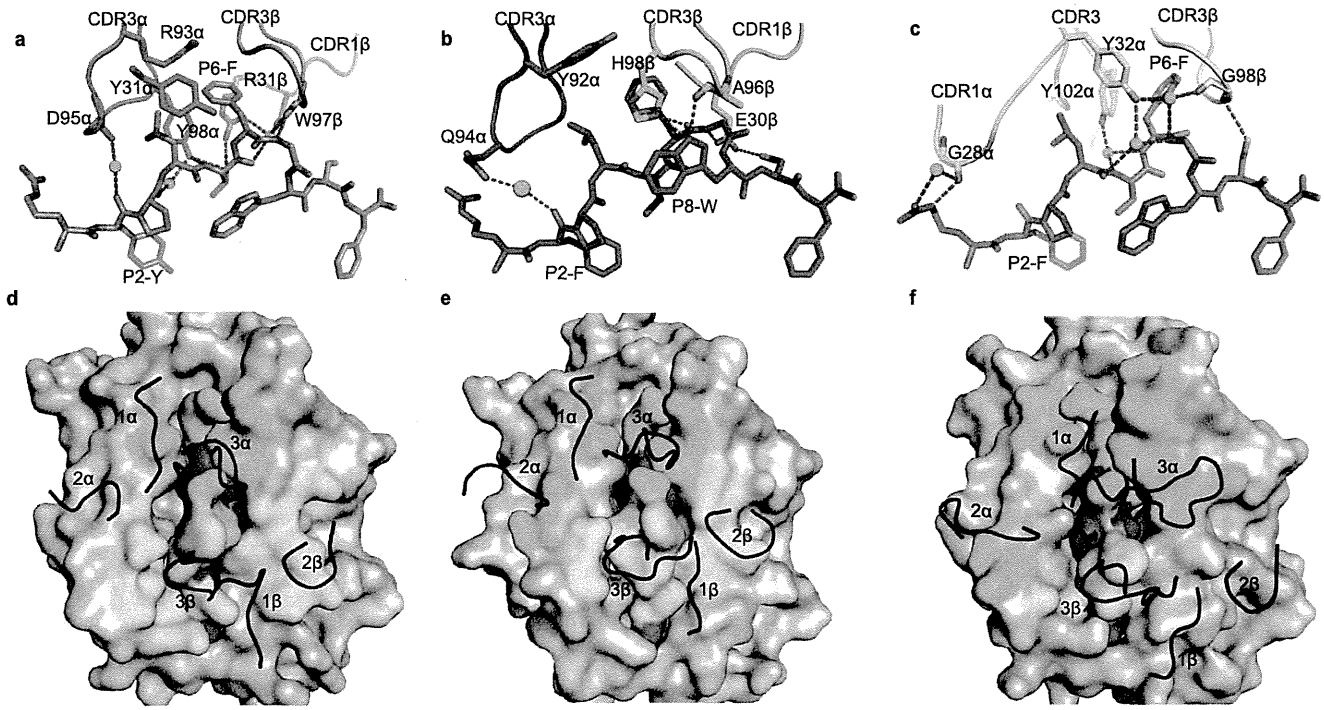


**Figure 3 | Comparisons of interaction of TCRs with pHLAs.** Binding interfaces: (a) the H27-14 TCR-A24/Nef134-10(wt), (b) the T36-5 TCR-A24/Nef134-10(2F) and (c) the C1-28 TCR-A24/Nef134-10(2F). TCRs are shown as loop representations and the residues important for binding with the peptide are represented as stick models. Nef134-10(wt), blue; Nef134-10(2F), red; water molecules, green spheres; hydrogen bonds, red dashed lines; water-mediated hydrogen bonds, blue dashed lines. pHLA surface representations with the binding footprint of TCRs: (d) H27-14 TCR with the A24/Nef134-10(wt), (e) T36-5 TCR with the A24/Nef134-10(2F) and (f) C1-28 TCR with the A24/Nef134-10(2F). The surfaces of pHLA interacted with TCR are shown in green for Vα and yellow for Vβ. The CDRs on the pHLAs are represented as black loops. HLA-A24, grey; Nef134-10(wt), blue; Nef134-10(2F), red.

and stayed until at least 2093 days after the initial visit. Notably, the 2nd position of Nef134-10 epitope was the wild type (Y) in all IMSUT cohort patients with F139L (Supplementary Fig. 6b). Although the number of patients with F139L was limited, the emergence of the mutation at position 139 suggests that the escape mechanism of the F139L mutant could be different from that of Y135F.

**Interaction between mutant- or dual-specific TCRs and A24/Nef134-10(2F).** Although Y135F has been described as an example of a CTL escape mutant in both epidemiological and immunological studies[10], A24/Nef134-10(2F) was recognized by T36-5 and by C1-28 (Fig. 1a and Table S3). Therefore, we decided to analyze the structure of TCR-A24/Nef134-10(2F) complexes in both mutant-specific T36-5 and dual-specific C1-28 TCRs.

Formation of T36-5-A24/Nef134-10(2F) introduced a large TCR-induced conformational change in the peptide, with insertion of H98β into a shallow pocket formed by L137(P4-L), F139(P6-F) and W141(P8-W) (Fig. 5a). Around this pocket, Y92α and Y31β were involved in the hydrophobic interactions with L137(P4-L) and F139(P6-F). In addition, H98β and S97β formed hydrogen bonds with the main chain of L137 (P4-L) and the side chain of W141(P8-W), respectively (Supplementary Table 3). As a consequence, the side chain of W141(P8-W), which was accommodated by HLA-A24 binding pocket in unligated state, moved about 5.6 Å shift toward TCR binding surface, forming a more exposed and featured peptide conformation. Thus, Nef134-10(2F) underwent large T36-5 TCR-induced conformational change affecting the main chain hydrogen bond networks within the peptide. In the unligated state, T138(P5-T) carbonyl formed two hydrogen bonds with the nitrogen atoms of G140(P7-G) and W141(P8-W); also the W141(P8-W) nitrogen formed a bond with the F139(P6-F) carbonyl (Fig. 5b). After the TCR ligation, the hydrogen bond between T138(P5-T) carbonyl and G140(P7-G) nitrogen was lost and T138 (P5-T) carbonyl reformed a single hydrogen bond with W141(P8-W) nitrogen (Fig. 5c).

C1-28 recognized Nef134-10(2F) and Nef134-10(wt) almost equally, while T36-5 recognized Nef134-10(2F) better than Nef134-10(wt). The extensive involvement of the Vα domain in the interaction of C1-28 TCR-A24/Nef134-10(2F) was unique and quite different from typical TCR-pHLA complexes (Fig. 3f). The extended tip of the non-germline-encoded CDR3α loop lay over the A24 α1-helix (65–69 residues); by contrast, the germline-encoded CDR1α loop interacted with the N-terminus of the Nef134-10(2F) peptide (Figs. 3f, 6a and Supplementary Fig. 7a). The framework residues of Vα8-3 had multiple interactions with HLA-A24: N-terminal A1α formed a hydrogen bond with E58, and R69α formed hydrogen bonds with A158, had VDW contacts with T163, and formed a water-mediated bond and salt bridges with D166 (Fig. 6a, c). In addition, CDR1α (Y27, G28, T30) and CDR2α (F51, S52) loops made multiple contacts with HLA-A24 residues (Fig. 6a, c and Supplementary Table 3). By contrast, Vβ4-1 made relatively few contacts with HLA-A24. S97 and I99 of the CDR3β interacted with HLA-A24 residues T73 and A150, respectively (Fig. 6b, d and Supplementary Table 3). In addition, S97β formed a water-mediated bond with the main chain of F139 (P6-F).

**Combination bias in the TCR variable gene segments used in dual-specific CTL.** We showed previously that Vα8-3 and Vβ4-1 were public TCRs used most frequently in the dual-specific CD8+ T cell population[14]. Many of the interactions with HLA-A24 described above could explain the bias for Vα8-3. We looked for the molecular clues for an exclusive use of Vβ4-1. Compared to the Vβ chains of H27-14 and T36-5 TCRs, Vβ4-1 sequences coded by the germline gene segments did not have much interaction with A24/Nef134-10(2F).

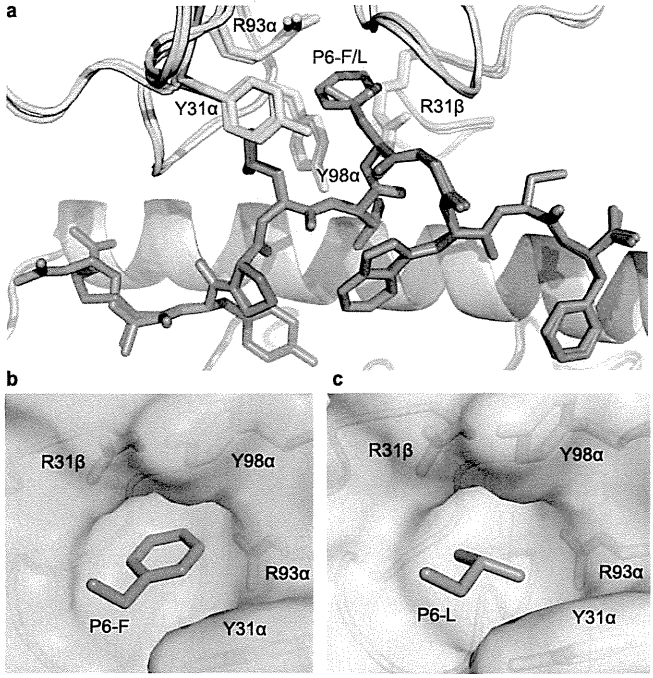


**Figure 4 | The pocket of H27-14 TCR surrounding Phe/Leu at position 6 of the Nef134-10 peptide.** (a) Overlay of the H27-14 TCR-A24/Nef134-10(wt) and H27-14 TCR-A24/Nef134-10(6L). The CDR loops in the H27-14 TCR in complex with A24/Nef134-10(wt) or A24/Nef134-10(6L) are shown in cyan or yellow, respectively. The Nef134-10(wt) or Nef134-10(6L) peptides are shown in blue or orange stick models, respectively. HLA-A24 α1 but not α2 helices are shown in grey cartoon representation for clarity. (b) The side chain of Phe at P6 (stick model in blue) is surrounded by the H27-14 TCR pocket formed by the CDR loops (cyan). (c) The side chain of Leu at P6 (stick model in orange) is surrounded by the H27-14 TCR pocket formed by the CDR loops (yellow).

The CDR2β loop in Vβ4-1 was displaced outside of HLA-A24 α1-helix by the CDR3α (Supplementary Fig. 7a, b). We reported previously that the GI (Gly-Ile) motif was present at position 98-99 of CDR3β loop in most dual-specific CD8+ T cell repertoire[14]. Interestingly, G98β formed a hydrogen bond with C142(P9-C) of the Nef134-10(2F) peptide and hydrophobic I99β interacted with hydrophobic A150 of the HLA-A24 (Fig. 6b, d and Supplementary Table 3).

HLA class I amino acid residues 65, 69, and 155, referred to as the restriction triad, are crucial for TCR recognition[18,19]. Although the types of contacts differed, all three TCRs solved in this study interact with the restriction triad (Supplementary Table 3). The tips of the CDR3α loop (residues 96-101) were sandwiched between HLA-A24 (G65 and A69) and Vβ (S55 and I56) in C1-28-A24/Nef134-10(2F); G98α and S55β formed hydrogen bonds with K68 of the HLA-A24 and S101α of the CDR3α, respectively (Fig. 6e). The presence of both S55β and I56β is unique to germline-encoded TRBV4-1 gene segment, and may contribute to stabilization between the CDR3α and the HLA-A24.

Although the CDR3α sequences (97–100 residues) of the public TCRs varied among dual-specific CTL clones[14], the sequences were composed of small amino acids such as Gly and Ser. For insertion into an interface between G65-A69 of the HLA-A24 and S55β-I56β and formation of stable interactions between the HLA-A24 complex and CDR3α residues, small size would be beneficial. Vβ4-1 may have been co-selected by geometric constraints imposed by Vα8-3 germline and hypervariable CDR3α sequences.

**The plasticity of Nef134-10 peptides.** In the interactions with HLA complexes, Nef134-10 peptides assumed an M-shaped conformation similar to the structure of the cancer-related telomerase peptide presented by HLA-A24 (Fig. 2a and 7a, b)[15]. The side chain of T138(P5-T) faced toward the groove of HLA-A24 and functioned as the secondary anchor residue (Fig. 2b). By switching the hydrogen bond from Y135(P2-Y)/H70 to T138(P5-T)/H70, the Y135(P2-Y) to 135F(P2-F) mutation maintained the conformation of the secondary anchor to HLA-A24 α1 helix. After TCR ligation, the C-terminus shifted more than the N-terminus in H27-14 TCR-A24/Nef134-10(wt) and T36-5 TCR/A24/Nef134-10(2F) (Fig. 7c). The main chain of F139(P6-F) shifted 2.81Å in H27-14 TCR-A24/Nef134-10(wt), and G140(P7-G) shifted 2.47Å in T36-5 TCR-A24/Nef134-10(2F). By contrast, C1-28 TCR-A24/Nef134-10(2F) had less shift in the main chain of the P5-P8 (0.32-0.74 Å) residues and greater shift of the P2-P4 residues (1.06–1.68 Å) in the N-terminus.

## Discussion

Nef134-10 epitope (RYPLTFGWCF) was a highly immunogenic epitope restricted by HLA-A24[10,14,20]. Y135F was the major escape mutation which appeared early in the clinical course (Supplementary Fig. 1a–c). Our previous study suggesting that Y135F was a processing mutation was later confirmed by others[10,21]. HIV-1 with Y135F mutation has been accumulating in the population with high HLA-A24 prevalence such as Japanese. Hence, Y135F is the ultimate escape mutation which appears early in the clinical course. F139L was a minor but also HLA-A24-related mutation. Intriguingly, all 6 patients with F139L mutation kept the wild type residue at 135$^{th}$ position in the epitope.

According to the crystal structure of the free wild type, A24/Nef134-10 epitope took M conformation epitope. L137(P4-L) and

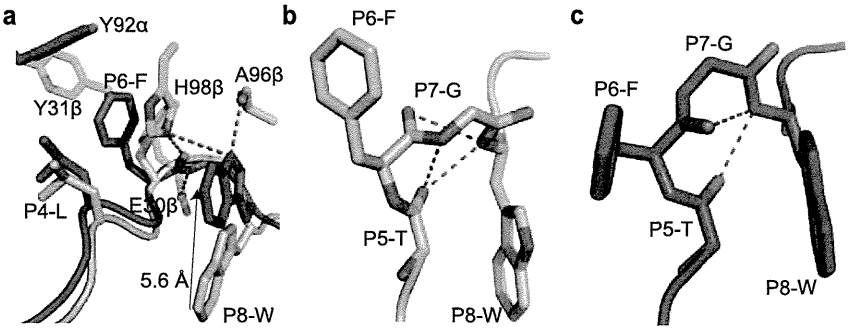


**Figure 5 | Interaction of T36-5 TCR with A24/Nef134-10(2F).** (a) pHLA unligated or ligated to T36-5 TCR. Nef134-10(2F) peptide of unligated pHLA, pink; the peptide ligated T36-5 TCR, red; CDRα, blue; CDRβ, green; hydrogen bonds, red dashed lines. (b) Peptide intramolecular hydrogen bonds in unligated pHLA. Color representation are the same as (a). (c) Peptide intramolecular hydrogen bonds in T36-5 TCR-A24/Nef134-10(2F) complex. Color representation are the same as (a).

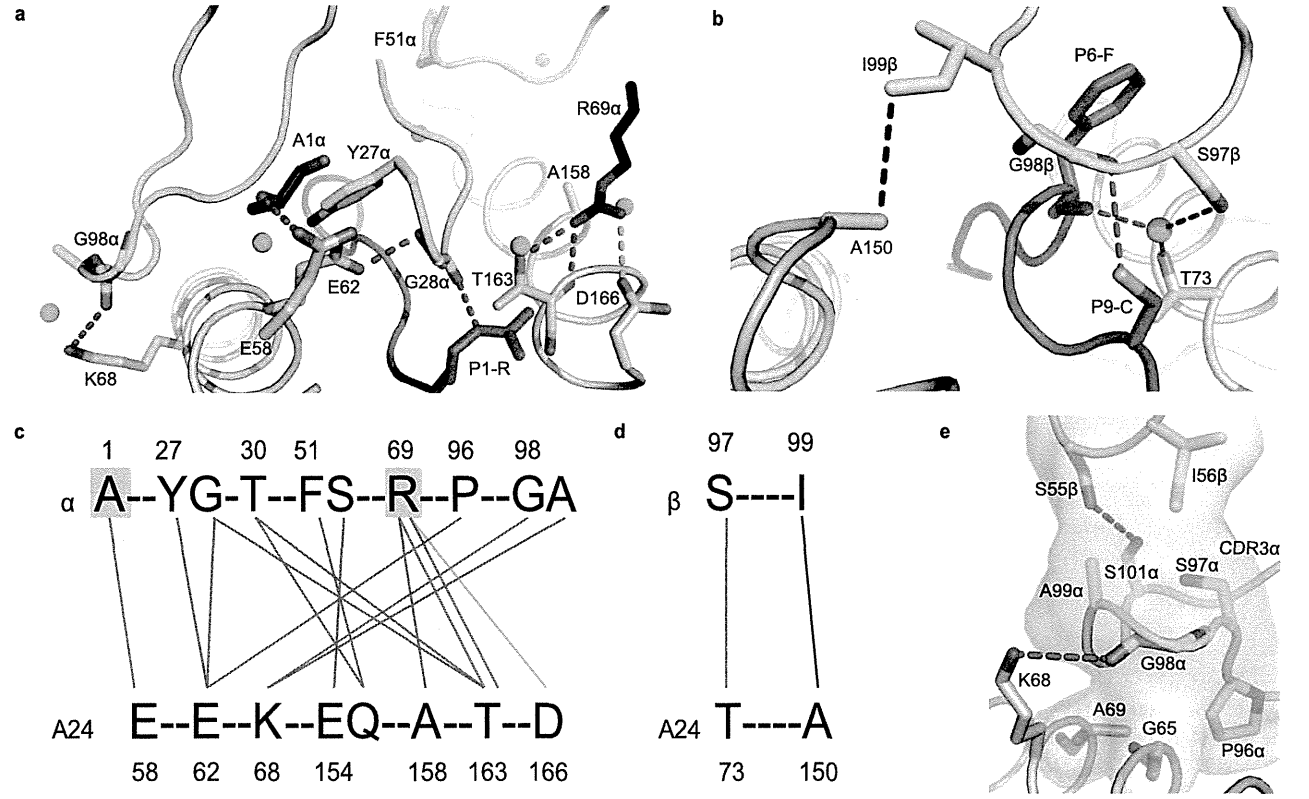


**Figure 6 | Interaction of C1-28 TCR with A24/Nef134-10(2F).** (a) Interaction of Vα and (b) Vβ with A24/Nef134-10(2F). CDRα, cyan; Fwα (Frame work region of Vα), black; CDR3β, yellow; Nef134-10(2F), red; HLA-A24, grey, water molecules, green spheres; red dashed lines, hydrogen bonds; a green dashed line, a salt bridge. Van der Waals contact (<4.0 Å), which is represented as a black dashed line, is shown in (b), but not in (a) for clarity. (c) Interactions of Vα and (d) Vβ with A24/Nef134-10(2F). Red, blue, green and black solid lines indicate hydrogen bonds, water-mediated hydrogen bonds, a salt bridge and van der Waals contact, respectively. Fwα residues (A1 and R69) are highlighted in grey. (e) For the C1-28 TCR, interactions of the tip of the CDR3α loop (residues 96-101, cyan) with S55β and I56β residues of the Vβ4-1 segments (yellow), and G65 and A69 residues of the HLA-A24 (grey). Red dashed lines indicate a hydrogen bond.

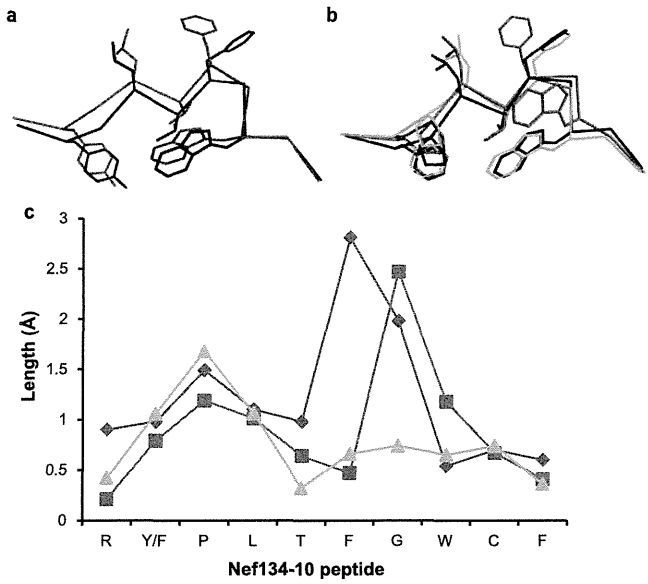


**Figure 7 | Structural change of the Nef134-10 peptides in free and TCR-bound states.** (a) Free Nef134-10(wt) (black) and Nef134-10(wt) bound to the H27-14 TCR (blue). (b) Free Nef134-10(2F) (black), the Nef134-10(2F) bound to T36-5 TCR (red) and the Nef134-10(2F) bound to the C1-28 TCR (green). (c) The migration length of the Nef134-10 main chain after TCR ligation, when HLA-A24 binding groove is superimposed.

F139(P6-F) were the eminent feature of this epitope and Y138(P5-T) was located in the valley of L137(P4-L) and F139(P6-F). N-terminal anchor, Y135(P2-Y), formed a hydrogen bond with His70 of HLA-A24 molecule. Although Y135F mutation interrupted this hydrogen bond, T138(P5-T) acted like a subanchor forming a hydrogen bond with HLA-A24 His70 keeping the M conformation very similar to the wild type. It should be noted that F is the 2nd best N-terminal anchor residue after Y for HLA-A24[22,23]. F139L mutation did not cause gross conformational change in the epitope, however, the solvent accessible surface area of the side chain became substantially smaller by the mutation. Namely, the epitope became slightly featureless by F139L mutation.

H27-14 TCR was highly specific to the wild type epitope ($K_D$ = 9.7 ± 0.7). Crystal structure of the complex was typical TCR/pMHC interaction in which CDR loops of α and β chains contributed almost equally to interact with the eminent feature of the epitope, F139(P6-F) residue. The binding affinity against early/major Y135F mutation diminished to nonfunctional level ($K_D$ = 291.5 ± 63.8). Although H27-14 TCR kept moderate affinity against F139L ($K_D$ = 64.8 ± 3.4), its TCR pocket was a better fit for bulky side chain of F139(P6-F) than for small side chain of 139L(P6-L). These findings may suggest that CTL with H27-14 TCR clonotype could contribute to eliminate HIV-1 with the wild type epitope but might be responsible for selection of viruses with the late/minor F139L mutation *in vivo*.

Nef134-10(2F)-specific T36-5 TCR had a very high affinity to A24/Nef134-10(2F) and extensive interaction shown by the BSA (approximately 2200 Å$^2$). The side chain of 141W(P8-W) was accommodated by the HLA-A24 binding cleft in the undocked state;

however, it was apparently lifted up by T36-5 TCR. Fujiwara et al. described CTL clones which recognized A24/Nef134-10(2F) more efficiently than the wild type (A24/Nef134-10(wt)). T36-5 may be one of those clones[21].

In the great majority of HLA-A24-positive chronically infected patients, plasma viruses had Y135F mutation, while the patients harbored dual specific CD8+ T cell population with highly restricted TCR repertoire[14]. The dual-specific CD8+ T cell population expressed higher activation markers such as PD1 than the wild type-specific CD8+ T cell population (Kawana-Tachikawa, A., unpublished observation). Puzzled by the presence of dual-specific CD8+ T cell population stimulated by the epitope with the processing mutation, we wished to study the molecular interaction between the TCR and pMHC. C1-28 was chosen for the structural study as the representative of the dual-specific CD8+ T cell population. As far as we know, this is the first report of the crystal structure of Vα8-3.

According to the structural analysis of dominant public TCRs, germline residues either of the Vβ or Vα may play a major role[24,25]. In C1-28 TCR, Vα domains contributed predominantly (80%) in the interaction with A24/Nef134-10(2F). N-terminal A1α, R69α, residues in CDR1α (Y27, G28, T30) and CDR2α (F51, S52) had multiple interactions with HLA-A24. Nongermline CDR3α loop (residues 96-101) also contributed to interact with the two residues of restriction triad in HLA-A24, while S101α had a hydrogen bond with S55β, a germline residue of public Vβ4-1. Therefore, hypervariable CDR3α contributed to bridge the binding of HLA-A24 and Vβ4-1. In terms of the interaction with the Nef134-10(2F) peptide, germline-encoded CDR1α loop (G28α) interacted with the N-terminus of the peptide 134R(P1-R). Also, hydroxyl groups of Y32 of CDR1α and Y102 of non-germline-encoded CDR3α made water-mediated bonds with the main chain of the peptide, while both aromatic rings made hydrophobic interaction with the aromatic ring of F139 (P6-F). Thus, CDR1α and CDR3α provided a major role in interaction with the Nef134-10(2F) in addition to the interaction with HLA-A24.

Compared to the other two TCRs examined in this study, the role of Vβ4-1 of the C1-28 TCR in the recognition of HLA-A24 and the peptide was not impressive. The CDR2β loop was displaced outside of the HLA-A24 α1-helix (residues 65–69) by the CDR3α of Vα8-3. However, S55β and I56β, germline residues unique to Vβ4-1, could contribute to stabilize the tip of CDR3α, which had an important interaction with the restriction triad. Thus, the major cause of the co-selection of Vβ4-1 as a public TCR could be the bias brought by the extensive interaction of the germline Vα8-3 residues with HLA-A24. In addition, the interaction of the small residues such as Gly and Ser in CDR3α with restrictive elements in the HLA-A24 contributed to the selection of Vβ4-1. Non-germline CDR3β contributed to the interaction with HLA-A24 (T73 and A150) and C142(P9-C) of the peptide. Collectively, these structural analyses revealed that T36-5 and C1-28 TCRs have their own unique mode of binding to a mutated epitope. The three TCRs studied did not introduce a substantial conformational change in the N-terminal side of the peptide; however, two TCRs with antigen preference but not the dual-specific C1-28 TCR introduced a large conformational change in the C-terminal side.

Recently, TCR/pMHC structure of KK10 epitope restricted by HLA-B*2705 was reported[26]. Clone C12C was cross-reactive to both wild type and early appearing Leu268Met mutant. Although both C12C and C1-28 were dually specific to both wild type and early mutant, the character of early mutation and their TCR/pMHC structure were quite different. In the case of KK10 epitope restricted by HLA-B*2705, Leu268Met was an early mutation affecting TCR recognition and the ultimate mutations such as Arg264Lys disrupting antigen presentation follow later. However, in the case of Nef134-10 epitope restricted by HLA-A24, early Y135 mutation was the ultimate mutation. Although the number of patients are still limited, late mutation in Nef134-10 epitope, F139L, occurred only in the patients without early/ultimate Y135F mutation. It is interesting to note that HLA-B*27 is a protective but HLA-A24 is not for the disease progression after HIV-1 infection[27]. Although further study is needed, the different mode of mutant appearance between HLA-B*2705/KK10 and HLA-A24/Nef134-10 epitopes may be related to the role of the HLA alleles on the disease progression.

In the population with high HLA-A24 prevalence, HIV-1 with the wild type Nef134-10 epitope is replaced by the virus with Y135F mutation early after infection. Or HIV-1 with Y135F may infect HLA-A24-positive people. Whichever the case, HIV-1 with Y135F mutation replicate for many years in the presence of activated dual-specific CTL. It is tempting to speculate that the Y135F mutation could be an example of "stealth mutation." HIV-1-infected cells might not be detected by specific- or dual-specific CTL due to processing failure or excess processing. If there is a difference in antigen processing between professional antigen presenting cells and infected T cells, CTL with functional TCR might be kept activated through cross-priming by professional antigen-presenting cells[28,29]. If this is the case, the immune system cannot see the infected cells as targets but may be kept activated by the spurious epitope presented by the uninfected professional antigen presenting cells. Although this hypothesis must be proven by further studies, our findings support the possibility that drugs which alter virus-peptide processing may have potential as "therapeutic vaccines."

## Methods

**Approval of the study and recombinant DNA experiments in IMSUT.** Plasma samples from HIV-1-positive patients attending the hospital affiliated with the Institute of Medical Science, the University of Tokyo (IMSUT) were collected and kept frozen until use. Patients provided written informed consent, and the study was approved by the Institutional Review Board of the University of Tokyo (approval number 20–31). Recombinant DNA experiments used in this work were approved by the Institutional Review Board (approval number 08–30).

**British columbia HOMER cohort.** Founded in 1996, the British Columbia HOMER cohort is an open cohort of antiretroviral-naïve, chronically HIV-1 infected individuals. The cohort is predominantly Caucasian. Plasma HIV-1 RNA sequencing and HLA class I sequence-based typing have been performed in the HOMER cohort as described[30]. Here, we investigated the relationship between HLA-A*24 expression and sequence variants at Nef codons 135 and 139 in 1018 HOMER participants with HIV-1 Nef and HLA-A data available.

**Longitudinal acute/early infection cohort.** A total of 16 HLA-A*24 expressing individuals from a longitudinal multicenter acute/early HIV-1 infection cohort were investigated to determine the time course of selection of sequence variants at Nef codons 135 and 139 using Kaplan-Meier methods as described in[11]. "Time to escape" was defined as the number of days elapsed between estimated infection date and first detection of the escape variant (as a full or partial amino acid change).

**Sequencing of autologous viruses.** Viral RNA from EDTA-treated plasma was isolated using the QIAamp viral RNA Mini kit (QIAGEN). For heparin-treated plasma, High Pure Viral Nucleic Acid Kit (Roche) was used for RNA isolation to remove the inhibitory effect of heparin on the PCR assay. HIV-1 *nef* region was amplified from the RNA using the Superscript III one-step RT-PCR system with Platinum Taq DNA polymerase with High Fidelity (Invitrogen) and *nef* specific primers. The second-round DNA-PCR was done with EX Taq DNA polymerase Hot Start enzyme (Takara). The sequences of primers for the above PCR reactions are available upon request. Purified PCR products were directly sequenced by using BigDye Terminator v3.1 Cycle Sequencing Kit (Applied Biosystems) on an ABI 3130xl Genetic Analyzer.

**Peptides.** Synthetic peptides of Nef134-10(wt) [RYPLTFGWCF], Nef134-10(2F) [RFPLTFGWCF] and Nef134-10(6L) [RYPLTLGWCF] were purchased from Sigma-Genosys.

**Generation of CTL clones.** Nef134-10-specific CTL clones were established from peripheral mononuclear cells (PBMCs) derived from HIV-1 infected individuals carrying the HLA-A*2402, as previously described[13].

**Sequencing of T-cell receptor α- and β-chains.** Analysis of genes encoding TCR α- and β-chains from cloned CTL were done as previously described[14].

**$^{51}$Cr release assay.** Cytotoxicity was measured by a standard $^{51}$Cr release assay as previously described[10].

**Protein expression and purification.** The H27-14, T36-5 and C1-28 TCRs were expressed, refolded and purified essentially as described[16]. For the H27-14 TCR refold, 24 mg of solubilized TCR α-chains and 20 mg of β-chains were injected into 1 L of a buffer containing 5 M urea, 100 mM Tris, pH 8.5, 400 mM L-arginine-HCl, 3.7 mM cystamine, 6.6 mM cysteamine, 0.2 mM PMSF (phenylmethylsulfonyl fluoride) at 4°C. The refolding solution was dialyzed twice for 24 h against 10 vol of milli Q water, and then 10 vol of 10 mM Tris, pH 8.5 at 4°C. The refolded TCR was then purified by Resource-Q column and Superdex 75 column (GE Healthcare). For the T36-5 TCR, 50 mg of α-chains and 40 mg of β-chains were refolded and purified as described above. For the C1-28 TCR refold, 20 mg of TCR α-chains and 35 mg of β-chains were injected twice into 2 L of a buffer containing 5 M urea, 100 mM Tris, pH 8.9, 400 mM L-arginine-HCl, 2 mM EDTA, 5 mM reduced glutathione, 0.5 mM oxidized glutathione, 0.2 mM PMSF at 4°C. After 24 hr incubation, the refolding solution was dialyzed twice for 24–36 h against 5 mM Tris, pH 8.5, 50 mM NaCl, and then 10 mM Tris, pH 8.5, 50 mM NaCl at 4°C. The resultant was purified by Resource-Q column, Mono-Q column and Superdex 75 column (GE Healthcare).

**Preparation of pHLAs.** The HLA-A*2402 heavy chain, HLA-A*2402 heavy chain-BSP (BirA substrate peptide) and β2 microglobulin (β2m) were also expressed separately in E. coli, as described[15]. For a 1 L refold, 45 mg of solubilized HLA-A*2402 heavy chains and 15 mg of β2m were injected into a refold buffer containing 100 mM Tris, pH 8.0, 400 mM L-arginine-HCl, 2 mM EDTA, 5 mM reduced glutathione, 0.5 mM oxidized glutathione, 0.2 mM PMSF in the presence of 10 mg of HIV-1 Nef 134-10 (wt), Nef134-10(2F) or Nef134-10 (6L) peptide. The refolded protein was purified by Superdex 75 column and MonoQ column. For SPR analysis, pHLA molecules were refolded in the same way as the above, using the HLA-A*2402-BSP instead of the HLA-A*2402 heavy chain. The pHLA-BSP was biotinylated as previously described[14].

**Surface plasmon resonance.** Surface plasmon resonance experiment was carried out at 25°C using BIAcore 2000 in a buffer containing 10 mM HEPES, pH 7.4, 150 mM NaCl, 3 mM EDTA, 0.005% Surfactant P20. Biotinylated pHLAs were immobilized to Sensor chip SA until the response was reached between 200–800 response units (RU). Each TCR was injected over the flow cells at a flow-rate of 20–30 μl/min with an indicated concentration range for equilibrium analysis. BIAevaluation software (version 4.1; GE healthcare) was used for data analysis. For kinetic analysis, 1 : 1 Langmuir binding model was used to calculate the $K_{on}$ and $K_{off}$ values.

**Crystallization and data collection.** All crystallizations were done by the sitting drop vapor diffusion method with a protein/reservoir drop ratio of 1 : 1 at 20°C. Crystallization conditions of grown crystals are shown in Supplementary Table S3. For cryoprotection, obtained crystals were soaked briefly and sequentially in reservoir solutions containing 10% and 20% ethylene glycol, and then flash-frozen in liquid nitrogen. Data were collected at the beamline BL41XU in SPring 8 (Hyogo, Japan) and BL-5A, NW12A and BL1A in the PF facility (Tsukuba, Japan), and processed with HKL2000[31] and the CCP4 program suite[32].

**Structure determination and refinement.** The structures were determined by molecular replacement using Molrep[33]. Search models used for molecular replacement were shown in Supplementary Table S3. Model building and refinement were conducted using Coot[34] and CNS 1.3[35], respectively. The further rounds of these refinements were performed using REFMAC implemented in CCP4. For building model of the T36-5 TCR-A24/Nef134-10(2F), diffraction intensities from the various crystals exhibited twin with an estimated twinning fraction of 0.45–0.49. Therefore, this structural model was refined using CNS 1.3 as a perfect twin.

The stereochemistry of the refined models was assessed with program Rampage[36]. All molecular graphics representations were created with the program PyMOL (DeLano Scientific; http://www.pymol.org). Data collection and refinement statistics are shown in Supplementary Table 2.


1. Kappler, J. *et al.* The major histocompatibility complex-restricted antigen receptor on T cells in mouse and man: identification of constant and variable peptides. *Cell* **35**, 295–302 (1983).
2. Marrack, P., Shimonkevitz, R., Hannum, C., Haskins, K. & Kappler, J. The major histocompatibility complex-restricted antigen receptor on T cells. IV. An antiidiotypic antibody predicts both antigen and I-specificity. *J Exp Med* **158**, 1635–1646 (1983).
3. McMichael, A. J. & Rowland-Jones, S. L. Cellular immune responses to HIV. *Nature* **410**, 980–987 (2001).
4. Walker, B. D. & Burton, D. R. Toward an AIDS vaccine. *Science* **320**, 760–764 (2008).
5. de la Salle, H. *et al.* Homozygous human TAP peptide transporter mutation in HLA class I deficiency. *Science* **265**, 237–241 (1994).
6. Fruh, K. *et al.* A viral inhibitor of peptide transporters for antigen presentation. *Nature* **375**, 415–418 (1995).
7. Maeurer, M. J. *et al.* Tumor escape from immune recognition: lethal recurrent melanoma in a patient associated with downregulation of the peptide transporter protein TAP-1 and loss of expression of the immunodominant MART-1/Melan-A antigen. *J Clin Invest* **98**, 1633–1641 (1996).
8. Bjorkman, P. J. *et al.* Structure of the human class I histocompatibility antigen, HLA-A2. *Nature* **329**, 506–512 (1987).
9. Davis, M. M. & Bjorkman, P. J. T-cell antigen receptor genes and T-cell recognition. *Nature* **334**, 395–402 (1988).
10. Furutsuki, T. *et al.* Frequent transmission of cytotoxic-T-lymphocyte escape mutants of human immunodeficiency virus type 1 in the highly HLA-A24-positive Japanese population. *J Virol* **78**, 8437–8445 (2004).
11. Brumme, Z. L. *et al.* Marked epitope- and allele-specific differences in rates of mutation in human immunodeficiency type 1 (HIV-1) Gag, Pol, and Nef cytotoxic T-lymphocyte epitopes in acute/early HIV-1 infection. *J Virol* **82**, 9216–9227 (2008).
12. Itoh, Y. *et al.* High-throughput DNA typing of HLA-A, -B, -C, and -DRB1 loci by a PCR-SSOP-Luminex method in the Japanese population. *Immunogenetics* **57**, 717–729 (2005).
13. Kawana-Tachikawa, A. *et al.* An efficient and versatile mammalian viral vector system for major histocompatibility complex class I/peptide complexes. *J Virol* **76**, 11982–11988 (2002).
14. Miyazaki, E. *et al.* Highly restricted T-cell receptor repertoire in the CD8+ T-cell response against an HIV-1 epitope with a stereotypic amino acid substitution. *AIDS* **23**, 651–660 (2009).
15. Cole, D. K. *et al.* Crystal structure of HLA-A*2402 complexed with a telomerase peptide. *Eur J Immunol* **36**, 170–179 (2006).
16. Boulter, J. M. *et al.* Stable, soluble T-cell receptor molecules for crystallization and therapeutics. *Protein Eng* **16**, 707–711 (2003).
17. Rudolph, M. G., Stanfield, R. L. & Wilson, I. A. How TCRs bind MHCs, peptides, and coreceptors. *Annu Rev Immunol* **24**, 419–466 (2006).
18. Tynan, F. E. *et al.* T cell receptor recognition of a 'super-bulged' major histocompatibility complex class I-bound peptide. *Nat Immunol* **6**, 1114–1122 (2005).
19. Burrows, S. R. *et al.* Hard wiring of T cell receptor specificity for the major histocompatibility complex is underpinned by TCR adaptability. *Proc Natl Acad Sci U S A* **107**, 10608–10613 (2010).
20. Ikeda-Moore, Y. *et al.* Identification and characterization of multiple HLA-A24-restricted HIV-1 CTL epitopes: strong epitopes are derived from V regions of HIV-1. *J Immunol* **159**, 6242–6252 (1997).
21. Fujiwara, M. *et al.* Different abilities of escape mutant-specific cytotoxic T cells to suppress replication of escape mutant and wild-type human immunodeficiency virus type 1 in new hosts. *J Virol* **82**, 138–147 (2008).
22. Ibe, M. *et al.* Role of strong anchor residues in the effective binding of 10-mer and 11-mer peptides to HLA-A*2402 molecules. *Immunogenetics* **44**, 233–241 (1996).
23. Sidney, J., Southwood, S. & Sette, A. Classification of A1- and A24-supertype molecules by analysis of their MHC-peptide binding repertoires. *Immunogenetics* **57**, 393–408 (2005).
24. Kjer-Nielsen, L. *et al.* A structural basis for the selection of dominant alphabeta T cell receptors in antiviral immunity. *Immunity* **18**, 53–64 (2003).
25. Stewart-Jones, G. B., McMichael, A. J., Bell, J. I., Stuart, D. I. & Jones, E. Y. A structural basis for immunodominant human T cell receptor recognition. *Nat Immunol* **4**, 657–663 (2003).
26. Ladell, K. *et al.* A molecular basis for the control of preimmune escape variants by HIV-specific CD8+ T cells. *Immunity* **38**, 425–436 (2013).
27. O'Brien, S. J., Gao, X. & Carrington, M. HLA and AIDS: a cautionary tale. *Trends Mol Med* **7**, 379–381 (2001).
28. Lehner, P. J. & Cresswell, P. Recent developments in MHC-class-I-mediated antigen presentation. *Curr Opin Immunol* **16**, 82–89 (2004).
29. Nakayama, K. *et al.* Imbalanced Production of Cytokines by T Cells Associates with the Activation/Exhaustion Status of Memory T Cells in Chronic HIV Type 1 Infection. *AIDS Res Hum Retroviruses* **28**, 702–714 (2011).
30. Brumme, Z. L. *et al.* Evidence of differential HLA class I-mediated viral evolution in functional and accessory/regulatory genes of HIV-1. *PLoS Pathog* **3**, e94 (2007).
31. Otwinowski, Z. & Minor, W. Processing of X-Ray Diffraction Data Collected in Oscillation Mode Macromolecular Crystallography. *Methods in Enzymology* **276**, 307–326 (1997).
32. The CCP4 suite: programs for protein crystallography. *Acta Crystallogr D Biol Crystallogr* **50**, 760–763 (1994).
33. Vagin, A. & Teplyakov, A. MOLREP: an Automated Program for Molecular Replacement. *J Appl Cryst* **30**, 1022–1025 (1997).
34. Emsley, P. & Cowtan, K. Coot: model-building tools for molecular graphics. *Acta Crystallogr D Biol Crystallogr* **60**, 2126–2132 (2004).
35. Brunger, A. T. *et al.* Crystallography & NMR System: A New Software Suite for Macromolecular Structure Determination. *Acta Cryst.* **D54**, 905–921 (1998).
36. Lovell, S. C. *et al.* Structure validation by Calpha geometry: phi,psi and Cbeta deviation. *Proteins: Structure, Function, and Genetics* **50**, 437–450 (2003).


## Acknowledgments

We thank the beam-line staffs at NW12A, BL1A and BL5A of Photon Factory (Tsukuba, Japan) and BL41XU of SPring8 (Hyogo, Japan) for technical help during data collection. We thank Drs. Richard Harrigan, Heiko Jessen, Anthony Kelleher, Martin Markowitz and Bruce Walker for specimen and/or data access. This work was supported in part by a contract research fund from the Ministry of Education, Culture, Sports, Science and Technology(MEXT)for Program of Japan Initiative for Global Research Network on Infectious Diseases (10005010)(AI); Global COE Program (Center of Education and Research for Advanced Genome-Based Medicine - For personalized medicine and the

control of worldwide infectious diseases-) of MEXT (F06)(AI); JSPS KAKENHI (25293226)(AKT); Grants for AIDS research from the Ministry of Health, Labor, and Welfare of Japan (H24-AIDS-IPPAN-008)(AKT); Research on international cooperation in medical science, Research on global health issues, Health and Labour Science Research Grants, the Ministry of Health, Labor, and Welfare of Japan (H25-KOKUI-SITEI-001)(AI); CJB is supported by a Vanier Canada Graduate Scholarship from the Canadian Institutes of Health Research (CIHR). EM is supported by a Master's Scholarship from the Canadian Association of HIV Research and Abbott Virology. ZLB is the recipient of a CIHR New Investigator Award and a Scholar Award from the Michael Smith Foundation for Health Research.

## Author contributions

A.S. did all the experiments from protein synthesis, BIAcore assay to structural studies. A.K.-T. did all the immunological studies including establishment of CTL cell lines and characterization of CTLs. A.Y. and Y.S. did crystallographic studies. C.Y.H. and D.Z. contributed to sequencing of viruses and TCR genes and analyzed the relationship between HLA-A*2402 expression and sequence variants at Nef codons 135 and 139 in IMSUT cohort. H.N. provided the clinical data of IMSUT cohort. T.K. was responsible for the clinical management in the IMSUT hospital. J.C. analyzed the relationship between HLA-A*2402 expression and sequence variants at Nef codons 135 and 139 in longitudinal multicenter acute/early HIV-1 infection cohort. E.M. and C.J.B. analyzed the relationship between HLA-A*24 expression and sequence variants at Nef codons 135 and 139 in British Columbia HOMER cohort. Y.S. discussed the structural study described in this manuscript. G.F.G. has been collaborating with A.I. and joined the discussion for this study. Z.L.B. investigated the relationship between HLA-A*24 expression and sequence variants at Nef codons 135 and 139 in 1018 participants in British Columbia HOMER cohort and longitudinal multicenter acute/early HIV-1 infection cohort with HIV-1 Nef and HLA-A data available. S.F. managed and instructed the structural study group and provided the environment for the crystallographic study and analysis. A.I. managed all the work described and wrote the manuscript. All authors reviewed the manuscript.

## Additional information

**Accession codes** C1-28 TCR/Nef134-10(2F), 3VXM; A24/Nef134-10(wt), 3VXN; A24/Nef134-10(2F), 3VXO; A24/Nef134-10(6L), 3VXP; H27-14 TCR, 3VXQ; H27-14 TCR-A24/Nef134-10(wt), 3VXR; H27-14 TCR-A24/Nef134-10(6L), 3VXS; T36-5 TCR, 3VXT; T36-5 TCR-A24/Nef134-10(2F), 3VXU and 3W0W.

**Supplementary information** accompanies this paper at http://www.nature.com/scientificreports

**Competing financial interests:** The authors declare no competing financial interests.

**How to cite this article:** Shimizu, A. *et al.* Structure of TCR and antigen complexes at an immunodominant CTL epitope in HIV-1 infection. *Sci. Rep.* 3, 3097; DOI:10.1038/srep03097 (2013).

REVIEW

# Cancer–infection interface in children after transplantation: posttransplant lymphoproliferative disorder and Epstein-Barr virus infection

*Mikiya Fujieda*[a] *and Motoshi Hattori*[b]

**Purpose of review**
To summarize the association between posttransplant lymphoproliferative disorder (PTLD), which is the most frequent cause of posttransplantation tumors in children, and Epstein–Barr virus (EBV) infection.

**Recent findings**
Most PTLD cases present as proliferation of EBV-infected B cells, because EBV-naive patients have no EBV-specific cytotoxic lymphocytes to control the infected cells. The monitoring of EBV loads in whole blood, as well as in plasma by PCR, represents a useful method for early diagnosis and timely treatment. A program of EBV control by molecular EBV monitoring coupled with lymphocyte phenotype analysis is recommended. Pre-emptive reduced immunosuppression may prevent PTLD, and improved therapeutic options may also contribute to milder PTLD phenotype and improved clinical course.

**Summary**
A recent trend is that PTLD incidence and high-grade histological findings have decreased because of appropriate immunosuppressive maintenance doses, monitoring of EBV, and preemptive treatment. More sensitive, specific tools for the detection of EBV replication and prophylactic methods are required to establish a definitive strategy for the prevention of PTLD after transplantation.

**Keywords**
Epstein–Barr virus, pediatric transplantation, PTLD

## INTRODUCTION

Posttransplant lymphoproliferative disorder (PTLD) is the most frequent cause of posttransplantation tumors in childhood. Early malignancies tend to be virus-related, such as PTLD [80% of cases caused by Epstein–Barr virus (EBV)] and Kaposi's sarcoma (caused by human herpes virus 8). Other viruses, such as human T-cell leukemia virus, cytomegalovirus (CMV), simian virus 40, and hepatitis C virus, may also increase the incidence of PTLD [1]. Pediatric transplant patients have a higher risk for PTLD than adults because many pediatric patients have never been exposed to EBV at transplantation and develop a primary EBV infection, a condition strongly associated with PTLD development [2].

The aim of this review is to summarize the association between EBV infection and PTLD, and discuss the risk factors, treatment, and prophylaxis, mainly in pediatric solid-organ transplantation (SOT).

## POSTTRANSPLANT LYMPHOPROLIFERATIVE DISORDER

The incidence of PTLD in pediatric recipients ranges from 0.46 to 30%, depending on the type of organ transplanted [3]. In the majority of cases, PTLD presents as abnormal proliferation of EBV-infected B cells [4], and its risk is highest during the first year after transplantation.

[a]Department of Paediatrics, Kochi Medical School, Kochi University, Kochi and [b]Department of Paediatric Nephrology, Kidney Center, Tokyo Women's Medical University, Tokyo, Japan

Correspondence to Mikiya Fujieda, MD, PhD, Department of Paediatrics, Kochi Medical School, Kochi University, Kohasu, Oko-cho, Nankoku, Kochi 783-8505, Japan. Tel: +81 88 880 2355; fax: +81 88 880 2356; e-mail: fujiedam@kochi-u.ac.jp

**Curr Opin Organ Transplant** 2013, 18:549–554
DOI:10.1097/MOT.0b013e3283651b0d

## KEY POINTS

- PTLD is the most frequent cause of posttransplantation tumor in childhood, and 80% of cases with PTLD is caused by EBV.
- Molecular EBV monitoring, coupled with lymphocyte phenotype analysis, is effective in controlling EBV infection.
- The recent trend in lower PTLD incidence and decreased high-grade histological findings is because of the use of lower immunosuppressants dose, the monitoring, and preemptive treatment of EBV.

### Risk factors and diagnosis of posttransplant lymphoproliferative disorder

The risk is lowest following renal transplantation (1–2%), moderate after heart, lung, and liver transplantation (3–12%), and highest after lung, small intestine, and multiorgan transplantation (up to 33%) [4]. PTLD is most common in intestinal or multiorgan transplant recipients because of the amount of lymphoid tissue that acts as a reservoir for EBV. A number of studies have reported that mammalian target of rapamycin (mTOR) inhibitors decreased the incidence of PTLD, but conflicting data have been derived from the recent observations [5▪]. New immunosuppressants, such as belatacept, tofacitinib, and efalizumab, have been observed to increase infectious complications, including PTLD, compared with cyclosporine [6–8].

EBV-seronegative recipients ($R^-$) who receive a transplant from EBV-seropositive donors ($D^+$) are at high risk [9,10▪]. The $R^-$ have no EBV-specific cytotoxic lymphocytes (CTLs) to control EBV. Analysis of the Organ Procurement and Transplantation Network/United Network for Organ Sharing database showed that the incidence of PTLD in donors and recipients who were both EBV-seronegative was very similar to that in the $D^+/R^-$ group, which may be explained by an increased chance of pediatric $R^-$ acquiring EBV after transplantation from other people [11▪]. Analysis of the Scientific Registry of Transplant Recipients in the USA revealed that $R^-$ had a higher PTLD risk not only after heart or kidney transplantation, but also after liver transplantation, even in recipients who were EBV-seropositive [12]. The reason is not known, but the larger lymphoid mass of the liver may favor EBV reactivation and progression to PTLD.

Patients with PTLD typically present with the evidence of peripheral adenopathy, hepatosplenomegaly, and tonsillitis, as well as diarrhea suggestive of gastrointestinal disease [13]. Because clinical symptoms may be scarce, the diagnosis should be considered in at-risk transplant recipients with fever lasting more than a few days without an identified source [13]. A tissue biopsy is needed for diagnosis, although specific tissue involvement may not be present, and in some patients, lesions may be inaccessible for biopsy. The WHO has classified PTLD into four categories: early lesions; polymorphous PTLD; monomorphic PTLD; and classical Hodgkin's lymphoma-type PTLD. Monomorphic PTLD is similar to lymphoma observed in nontransplant patients, with the vast majority being B-cell lymphoma [13].

### Monitoring of Epstein–Barr virus DNA load and lymphocyte phenotype, and other parameters

As the onset of PTLD is preceded by a preclinical phase characterized by elevated EBV load in the peripheral blood, monitoring of EBV DNA levels in the blood by PCR represents a useful tool for early diagnosis and timely treatment, although not every case of PTLD is associated with elevated EBV DNA [14–16]. In pediatric liver transplantation, EBV viremia was detected at $7.6 \pm 3.6$ days after transplantation in 27% of recipients, but did not affect the short-term outcome (during the first 21 days after transplantation) [17]. PTLD occurred in 11% of patients with peak EBV load of $10^3$–$10^5$ copies/ml vs. 37% of patients with levels greater than $10^5$ copies/ml. In addition, EBV PCR was predictive in 78% of patients tested within 3 weeks prior to the tissue diagnosis of PTLD [18]. Ruf *et al.* [19▪▪] reported that in pediatric patients after heart transplantation or allograft hematopoietic stem cell transplantation, routine screening of EBV DNA in whole blood appeared to be a useful tool supplemented by EBV load measurement in plasma to discriminate chronic high EBV load (CHL) carriers without the risk for PTLD from those who are at risk for PTLD. Values in whole blood higher than 20 000 copies/ml and plasma values higher than 1000 copies/ml indicated the presence of PTLD (whole blood: sensitivity 100%, specificity 87%; plasma: sensitivity 88%, specificity 98%) [19▪▪].

There are four EBV latency states in EBV-infected B cells [20▪▪] (Fig. 1). Three of these (latency I to latency III) are found in PTLD and each has different levels of immunogenicity, and a different type of lymphoma. In SOT recipients, usually within 6 months after transplantation, B cells expressing type III latency are frequently detected in lymph nodes. These may be categorized as lymphoid hyperplasia that frequently responds to reduced immune suppression (RIS). In some transplant cases, they

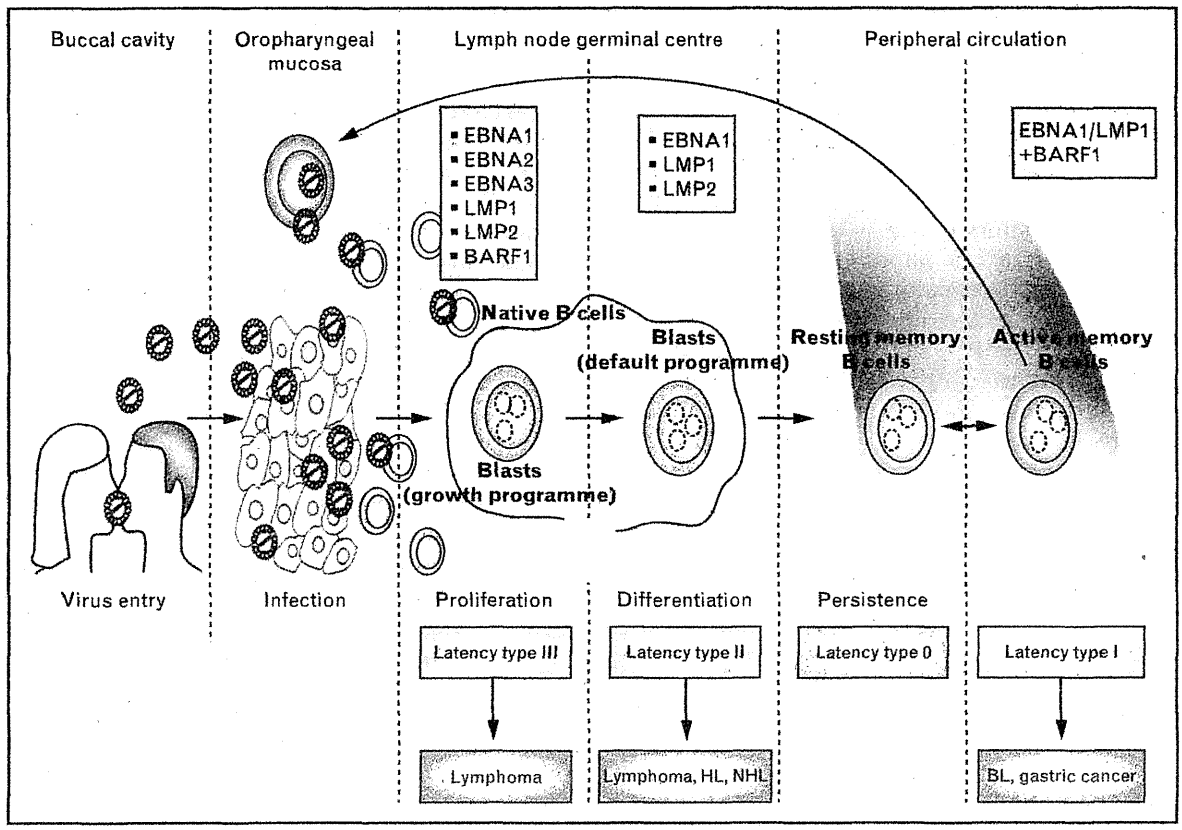


FIGURE 1. EBV latency stages and lymphoma. EBV-infected naive B cells express entire latency genes (type III). They enter lymphoid follicles and express only three viral proteins (type II). Finally, they exit the lymph nodes and downregulate all viral proteins (type 0). If circulating infected B cells divide homeostatically, they express a single viral protein (EBNA 1, type I). BL, Burkitt's lymphoma; EBV, Epstein–Barr virus; HL, Hodgkin's lymphoma; NHL, non-Hodgkin's lymphoma. Modified from [20▪▪].

may develop into diffuse large B-cell lymphoma [20▪▪,21]. This type of lymphoma is highly immunogenic, efficiently removed by EBV-CTLs, and never seen in immunocompetent individuals. In addition, pediatric renal transplant patients with CHL (5000 copies/ml whole blood, over 6 months) were seen to have expression of latent genes such as EB nuclear antigen (*EBNA*) 1, latent membrane protein (*LMP*) 1, *LMP2*, and the lytic gene *BZLF1* [22]. However, EBV gene-expression patterns were not associated with EBV DNA load, although one report described that *LMP1* and *LMP2* expression correlated with the viral load [21].

We reported that EBV-CTL specific to the EBV latent proteins (EBNA3A and EBNA3B) and lytic proteins (BRLF1 and BMLF1) were significantly lower in pediatric renal transplant recipients with PTLD and asymptomatic CHL (>1000 copies/μg DNA for over 6 months in peripheral mononuclear cells) compared with control when EBV loads first rose above 100 copies/μg DNA [9,23]. Imadome *et al.* [24▪▪] demonstrated that an increase in the number of $CD8^+HLA\text{-}DR^+$ cells was observed in parallel with a decrease in EBV load, and a dramatic increase in the number of EBV-CTL specific to *LMP2* was accompanied by a decline in EBV load in pediatric liver transplant recipients. These investigators proposed a program of EBV control by molecular EBV monitoring coupled with lymphocyte phenotype analysis [24▪▪]. Asymptomatic pediatric thoracic transplant patients have been observed to present significant expression of the $CD56^{bright}CD16^{\pm}$ subset and display effective EBV-specific natural killer cell function, whereas PTLD patients have been seen to accumulate $CD56^{dim}CD16^-$ and $CD56^-CD16^+$ subsets [25].

Elevated levels of both kappa and lambda immunoglobulin-free light chains (FLCs) (and a normal kappa/lambda FLC ratio) indicate polyclonal B-cell activation. A skewed FLC ratio is suggestive of the presence of an abnormal monoclonal B-cell population. Patients with PTLD after SOT have higher kappa and lambda FLC ratios. Using the samples obtained at an average of 3.5 months before PTLD

diagnosis, cases were likely to have elevated FLC levels. High EBV DNA loads in blood were associated with elevated FLC levels. FLC elevation is associated with heightened PTLD risk. The abnormal FLC ratio likely reflects B-cell dysfunction, perhaps related to EBV-driven lymphoproliferation [26▪]. The chemokine CXCL13 (B-cell attracting chemokine 1) is a CXC subtype member and acts via its receptor CXCR5. It plays a crucial role in B-cell homing and lymphoid organ development, and is expressed in some cases of lymphomatous disease. Pediatric SOT recipients with PTLD had higher serum CXCL13 levels than healthy controls and recipients with EBV reactivation. Elevated serum CXCL13 levels were detected up to 2 years prior to PTLD diagnosis and correlated with the response to RIS [27].

## Treatment for posttransplant lymphoproliferative disorder

When the diagnosis of PTLD is confirmed, it is imperative to consider RIS to the lowest tolerated levels (usually 25–50% of baseline) or even complete withdrawal as the first line of treatment, although there is wide variation in the response rate (as many as 23–100% of cases). Patients with monomorphic PTLD are less likely to respond [20▪▪]. A response to RIS is usually seen within 2–4 weeks [28], but if there is only a partial response or disease progression, further treatment is urgently required. On the other hand, the present authors and Imadome *et al.* have demonstrated that molecular EBV monitoring coupled with lymphocyte phenotype analysis is effective in controlling EBV infection with preemptive RIS [23,24▪▪].

Rituximab monotherapy has shown a good toxicity profile, but the response rate has been inadequate [13]. However, Gross *et al.* [29] reported that the 2-year event-free survival was 71% and overall survival was 83%, with a median follow-up of 4.8 years in 55 pediatric SOT recipients on a regimen of low-dose cyclophosphamide and prednisone. Worth *et al.* [30] reported the efficacy of a preemptive strategy based on the combination of EBV viremia (>40 000 copies/ml whole blood) and CD3 count ($<0.3 \times 10^9$/l) in preventing PTLD following T-cell-depleted stem cell transplantation.

Recent studies by Hatton *et al.* and others [31▪▪,32] have elucidated the cellular signaling pathway initiated by LMP1 and LMP2a in EBV-infected B cells. These two viral proteins act as mediators for the survival of EBV-infected B cells that are long lived. Both LMP1 and LMP2a activate Syk, then Syk activates the phosphatidylinositol 3-kinase (PI3K)/Akt/mTOR signaling pathway [31▪▪,32]. The development and testing of inhibitors of this signaling pathway may reveal new opportunities for the treatment of PTLD.

Antiherpes virus agents are dependent on intracellular phosphorylation by virally encoding thymidine kinase to become activated. Although EBV-transformed cells do not express thymidine kinase, antiviral prophylaxis with ganciclovir/valganciclovir has been associated with a significantly decreased incidence of EBV primary infection: 45% in the prophylaxis group compared with 100% of controls in EBV-naive pediatric renal transplant recipients in the first year after transplant [33].

EBV-associated PTLD usually expresses all latent EBV viral proteins and is therefore amenable to T-cell therapy such as donor lymphocyte infusion (DLI) and adoptive transfer of EBV-CTL. T-cell therapies, except DLI, are currently experimental and only available in the context of a clinical trial [20▪▪]. Future therapeutic strategies for PTLD may focus on the combinations of EBV-CTL and antibody therapy [20▪▪]. Such an approach has the potential to minimize the use of untargeted cytotoxic chemotherapy for patients, even those with advanced disease, thereby potentially not only preventing unacceptable cytotoxicities, but also enabling an improved outcome for patients with EBV-associated PTLD.

## Outcome of posttransplant lymphoproliferative disorder

A recent trend toward a reduction in overall PTLD incidence has been observed, particularly in EBV-seronegative recipients at transplantation [11▪,34,35▪]. Kerkar *et al.* [34] reported that 7.5% of pediatric liver transplant recipients in 2001–2005 (Era A) and 10.9% in 1993–1997 (Era B) were diagnosed with PTLD. Patients in Era A presented with significantly less advanced histological disease (hyperplastic/polymorphic PTLD) compared with patients in Era B (monomorphic PTLD). Three recipients in Era B died secondary to PTLD, whereas there were no PTLD-related deaths during Era A [34]. From a search of the National Israeli Kidney Transplant Registry for 2001–2008, Cleper *et al.* [35▪] found that PTLD developed in 12 of 272 (4.4%) pediatric renal transplant recipients at a median of 3.2 years after transplantation. Patients who were EBV-seronegative at transplantation developed PTLD earlier after transplantation compared with EBV-seropositive patients (1.9 vs. 6.3 years, respectively), and the former had B-cell type PTLD. Most significantly, survival was 100% in the EBV-seronegative patients with PTLD and 40% in the EBV-seropositive patients with PTLD [35▪].

The recent trend in the lower incidence of PTLD and the decrease in high-grade histological findings in pediatric transplant recipients may be explained by some reasons. First, lower immunosuppressive maintenance doses and a more rational use of induction agents diminish the number of complications related to over-immunosuppression. Second, these positive developments have been because of the monitoring of EBV and preemptive treatment. A possible third explanation is the use of prophylactic treatment or routine surveillance with preemptive treatment for other viruses, including CMV and BK virus.

## CONCLUSION

The recent trend in lower PTLD incidence and decreased high-grade histological findings are because of the use of lower immunosuppressive maintenance doses, the monitoring and preemptive treatment of EBV, and the use of prophylactic treatment or routine surveillance for other viruses. However, more sensitive, specific tools for the detection of EBV replication and prophylactic methods are required to establish a definitive strategy for the prevention of PTLD after transplantation in pediatric recipients.

## Acknowledgements

*None.*

## Conflicts of interest

*There are no conflicts of interest in connection with this article.*

## REFERENCES AND RECOMMENDED READING

Papers of particular interest, published within the annual period of review, have been highlighted as:

- ■ of special interest
- ■■ of outstanding interest

Additional references related to this topic can also be found in the Current World Literature section in this issue (pp. 611–613).

1. Vegso G, Hajdu M, Sebestyen A. Lymphoproliferative disorders after solid organ transplantation – classification, incidence, risk factors, early detection and treatment options. Pathol Oncol Res 2011; 17:443–454.
2. Nourse JP, Jones K, Gandhi MK. Epstein-Barr virus-related posttransplant lymphoproliferative disorders: pathogenetic insights for targeted therapy. Am J Transplant 2011; 11:888–895.
3. Schonder KS, Mazariegos GV, Weber RJ. Adverse effects of immunosuppression in pediatric solid organ transplantation. Pediatr Drugs 2010; 12:36–49.
4. Murukesan V, Murkherjee S. Managing posttransplant lymphoproliferative disorders in solid-organ transplant recipients: a review of immunosuppressant regimens. Drugs 2012; 72:1631–1643.
5. ■ Sampaio MS, Cho YW, Shah T, *et al.* Association of immunosuppressive maintenance regimens with posttransplant lymphoproliferative disorder in kidney transplant recipients. Transplantation 2012; 93:73–81.

This review from the OPTN/UNOS database discussed the incidence of PTLD and graft failure with various combinations of immunosuppressive agents.

6. Marks SD. New immunosuppressants in pediatric solid organ transplantation. Curr Opin Organ Transplant 2012; 17:503–508.
7. Vincenti F, Larsen CP, Alberu J, *et al.* Three-year outcomes from BENEFIT, a randomized, active-controlled, parallel-group study in adult kidney transplant recipients. Am J Transplant 2012; 12:210–217.
8. Pestana JO, Grinyo JM, Vanrenterghem Y, *et al.* Three-year outcomes from BENEFIT-EXT: a phase III study of belatacept versus cyclosporine in recipients of extended criteria donor kidneys. Am J Transplant 2012; 12:630–639.
9. Sato T, Fujieda M, Maeda A, *et al.* Monitoring of Epstein-Barr virus load and killer T cells in pediatric renal transplant recipients. Clin Nephrol 2008; 70:393–403.
10. ■ Chinnock R, Webber SA, Dipchand AI, *et al.* A 16-year multiinstitutional study of role of age and EBV status on PTLD incidence among pediatric heart transplant recipients. Am J Transplant 2012; 12:3061–3068.

This multiinstitutional study showed that EBV status and the time of transplantation are important variables in the development of PTLD in pediatric heart transplant recipients.

11. ■ Sampaio MS, Cho YW, Shah T, *et al.* Impact of Epstein-Barr virus donor and recipient serostatus on the incidence of posttransplant lymphoproliferative disorder in kidney transplant recipients. Nephrol Dial Transplant 2012; 27:2971–2979.

Using the OPTN/UNOS database, this article demonstrated the incidence of PTLD and mortality with respect to EBV serostatus, transplant type (deceased donor or living donor) and transplantation era.

12. Dharnidharka VR, Lamb KE, Gregg JA, Meier-Kriesche HU. Associations between EBV serostatus and organ transplant type in PTLD risk: an analysis of the SRTR National Registry Data in the United States. Am J Transplant 2012; 12:976–983.
13. Comoli P, Ginevri F. Monitoring and managing viral infections in pediatric renal transplant recipients. Pediatr Nephrol 2012; 27:705–717.
14. Sato T, Fujieda M, Tanaka E, *et al.* Monitoring of Epstein-Barr virus load and antibody in pediatric renal transplant patients. Pediatr Int 2008; 50:454–458.
15. Ishihara M, Tanaka E, Sato T, *et al.* Epstein-Barr virus load for early detection of lymphoproliferative disorder in pediatric renal transplant recipients. Clin Nephrol 2011; 76:40–48.
16. Shimizu H, Saitoh T, Koya H, *et al.* Discrepancy in EBV-DNA load between peripheral blood and cerebrospinal fluid in a patient with isolated CNS post-transplant lymphoproliferative disorder. Int J Hematol 2011; 94:495–498.
17. Indolfi G, Heaton N, Smith M, *et al.* Effect of early EBV and/or CMV viremia on graft function and acute cellular rejection in pediatric liver transplantation. Clin Transplant 2012; 26:E55–E61.
18. Holman CJ, Karger AB, Mullan BD, *et al.* Quantitative Epstein-Barr virus shedding and its correlation with the risk of posttransplant lymphoproliferative disorder. Clin Transplant 2012; 26:741–747.
19. ■■ Ruf S, Behnke-Hall K, Gruhn B, *et al.* Comparison of six different specimen types for Epstein-Barr viral load quantification in peripheral blood of pediatric patients after heart transplantation or after hematopoietic stem cell transplantation. J Clin Virol 2012; 53:186–194.

*This excellent study revealed that routine screening of EBV DNA in whole blood* appears to be a useful tool supplemented by EBV DNA load measurement in plasma to discriminate chronic high viral load carriers with a high risk for PTLD from those without the risk for PTLD among pediatric transplant recipients.

20. ■■ Bollard CM, Rooney CM, Heslop HE. T-cell therapy in the treatment of posttransplant lymphoproliferative disease. Nat Rev Clin Oncol 2012; 9: 510–519.

*This excellent review describes the EBV cycle, latency stages and lymphoma, and* current approaches to T-cell-based therapies such as adoptive transfer of EBV-CTL to treat PTLD and strategies that improve the feasibility of such treatment.

21. Kasztelewicz B, Jankowska I, Pawlowska J, *et al.* Epstein-Barr virus gene expression and latent membrane protein 1 gene polymorphism in pediatric liver transplant recipients. J Med Viol 2011; 83:2182–2190.
22. Moran J, Carr M, Waters A, *et al.* Epstein-Barr virus gene expression, human *leukocyte antigen alleles and chronic high viral loads in pediatric renal* transplant patients. Transplantation 2011; 92:328–333.
23. Tanaka E, Sato T, Ishihara M, *et al.* Asymptomatic high Epstein-Barr viral load carriage in pediatric renal transplant recipients. Pediatr Transplant 2011; 15:306–313.
24. ■■ Imadome K, Fukuda A, Kawano F, *et al.* Effective control of Epstein-Barr virus infection following pediatric liver transplantation by monitoring of viral DNA load and lymphocyte surface markers. Pediatr Transplant 2012; 16:748–757.

This excellent study revealed that EBV control by molecular EBV monitoring, coupled with lymphocyte analysis such as for $CD8^{-}HLA\text{-}DR^{+}$ cells or EBV CTL, is effective in controlling EBV infection in pediatric liver transplant recipients.

25. Wiesmayr S, Webber SA, Macedo C, *et al.* Decreased NKp46 and NKG2D and elevated PD-1 are associated with altered NK-cell function in pediatric transplant patients with PTLD. Eur J Immunol 2012; 42:541–550.
26. ■ Engels EA, Preiksaitis J, Zingone A, Landgren O. Circulating antibody free light chains and risk of posttransplant lymphoproliferative disorder. Am J Transplant 2012; 12:1268–1274.

The use of circulating antibody-free light chain levels in conjunction with EBV DNA load may help identify recipients at highest risk for PTLD, which would facilitate targeted interventions.

27. Schiffer L, Henke-Gendo C, Wilsdorf N, *et al.* CXCL13 as a novel marker for diagnosis and disease monitoring in pediatric PTLD. Am J Transplant 2012; 12:1610–1617.

28. Parker A, Bowles K, Bradley JA, *et al.* Management of posttransplant lymphoproliferative disorder in adult solid organ transplant recipients – BCSH and BTS guidelines. Br J Haematol 2010; 149:693–705.
29. Gross TG, Orjuela MA, Perkins SL, *et al.* Low-dose chemotherapy and rituximab for posttransplant lymphoproliferative disease (PTLD): a Children's Oncology Group Report. Am J Transplant 2012; 12:3069–3075.
30. Worth A, Conyers R, Cohen J, *et al.* Preemptive rituximab based on viraemia and T cell reconstitution: a highly effective strategy for the prevention of Epstein-Barr virus-associated lymphoproliferative disease following stem cell transplantation. Br J Haematol 2011; 155:377–385.
31. ■■ Hatton O, Martinez OM, Esquivel CO. Emerging therapeutic strategies for Epstein-Barr virus + posttransplant lymphoproliferative disorder. Pediatr Transplant 2012; 16:220–229.

This excellent review focuses on the oncogenic signaling pathways activated by the EBV LMP1 and LMP2a to understand the underlying mechanisms and mediators of lymphomagenesis, with the goal of identifying novel, rational therapeutic targets for the treatment of EBV-associated malignancies.

32. Hatton O, Phillips LK, Vaysberg M, *et al.* Syk activation of phosphatidylinositol 3-kinase/Akt prevents HtrA2-dependent loss of X-linked inhibitor of apoptosis protein (XIAP) to promote survival of Epstein-Barr virus+ ($EBV^+$) B cell lymphomas. J Biol Chem 2011; 286:37368–37378.
33. Höcker B, Böhm S, Fickenscher H, *et al.* (Val-)Ganciclovir prophylaxis reduces Epstein-Barr virus primary infection in pediatric renal transplantation. Transpl Int 2012; 25:723–731.
34. Kerkar N, Morotti RA, Madan RP, *et al.* The changing face of posttransplant lymphoproliferative disease in the era of molecular EBV monitoring. Pediatr Transplant 2010; 14:504–511.
35. ■ Cleper R, Ben Shalom E, Landau D, *et al.* Posttransplantation lymphoproliferative disorder in pediatric kidney-transplant recipients – a national study. Pediatr Transplant 2012; 16:619–626.

This study demonstrated that pretransplantation EBV-seronegative status might confer a survival benefit with early detected PTLD. Among pediatric kidney transplant recipients, EBV-seropositive patients are at risk for aggressive late-onset lethal PTLD.

JOURNAL OF SURGICAL RESEARCH 180 (2013) 349–355

Available online at www.sciencedirect.com

SciVerse ScienceDirect

journal homepage: www.JournalofSurgicalResearch.com

# Impact of endotoxin measured by an endotoxin activity assay during liver transplantation

*Yukihiro Sanada, MD,[a,*] Koichi Mizuta, MD, PhD,[a] Taizen Urahashi, MD, PhD,[a] Yoshiyuki Ihara, MD, PhD,[a] Taiichi Wakiya, MD,[a] Noriki Okada, MD,[a] Naoya Yamada, MD,[a] Kentaro Ushijima, PhD,[b] Shinya Otomo,[c] Koichi Sakamoto, PhD,[c] Yoshikazu Yasuda, MD, PhD,[d] and Hideo Kawarasaki, MD, PhD[a]*

[a] *Department of Transplant Surgery, Jichi Medical University, Shimotsuke City, Tochigi, Japan*
[b] *Department of Clinical Pharmacology, Jichi Medical University, Shimotsuke City, Tochigi, Japan*
[c] *Department of Pharmacy, Jichi Medical University Hospital, Shimotsuke City, Tochigi, Japan*
[d] *Department of Surgery, Jichi Medical University, Shimotsuke City, Tochigi, Japan*

ARTICLE INFO

*Article history:*
Received 11 December 2011
Received in revised form
29 April 2012
Accepted 2 May 2012
Available online 24 May 2012

*Keywords:*
Endotoxin activity assay
Endotoxin
Infection
Acute rejection
Liver transplantation

ABSTRACT

*Background:* Endotoxin (Et) in the portal vein blood is processed by the hepatic reticuloendothelial system. Thus, it is possible that the Et kinetics of the peripheral venous blood may be useful as a biological index that can be used to evaluate liver function. In this study, we measured Et using the endotoxin activity assay in peripheral venous blood during living donor liver transplantation (LDLT), to study its clinical significance.

*Methods:* Subjects were 17 patients who underwent LDLT. In the perioperative peripheral venous blood, was measured Et activity (EA) using the endotoxin activity assay at 1 or 2 d before LT, and then on 1, 5, 7, 14, and 21 postoperative days.

*Results:* Patients with infections had significantly higher EA levels compared with those without complications before LDLT and 14 postoperative days ($P = 0.038$ and 0.027, respectively). The average EA level of patients with infections and without complications before LT was 0.22 and 0.08, respectively ($P = 0.038$). Patients with an EA level higher than 0.20 before LDLT had a significantly longer period of hospitalization compared with those without complications ($P = 0.038$).

*Conclusions:* A preoperative EA level more than 0.20 is a high risk factor for post-transplant infection and a prolonged period of hospitalization.



## 1. Introduction

Endotoxin (Et) in the portal venous blood is processed by the hepatic reticuloendothelial system. Thus, if liver function decreases and processing cannot be performed, endotoxinemia may develop [1–3]. Therefore, it is possible that the Et kinetics in peripheral venous blood may represent a biological index that can be used to evaluate liver function.

It is believed that Et and cytokines in the field of liver transplantation (LT) are major factors that influence circulatory dynamics and ischemia reperfusion injury [4], and the Et kinetics during the perioperative period of LT can be

* *Corresponding author.* Department of Transplant Surgery, Jichi Medical University, 3311-1 Yakushiji, Shimotsuke City, Tochigi 329-0498, Japan. Tel.: +81 285 58 7069; fax: +81 285 58 7069.
E-mail address: yuki371@jichi.ac.jp (Y. Sanada).
0022-4804/$ – see front matter 
doi:10.1016/j.jss.2012.05.004

a biological index that sensitively reflects changes in graft liver function. Furthermore, through measurement of Et activity, rejection and infections can be differentiated or predicted [5], allowing for earlier diagnosis and treatment of such complications.

The endotoxin activity assay (EAA) was recently developed, which is capable of rapidly measuring Et levels by a chemiluminescence method using neutrophil activity [6,7]. The efficacy of this method has been demonstrated [5,8,9]. We previously reported that the EAA can be used to monitor hepatic clearance and to ascertain Et kinetics, because endotoxin activity (EA) determined using the EAA also reflects hepatic clearance in a manner similar to beta-D-glucan and $NH_3$ [10]. Therefore, it may be useful to employ the EAA during the course of LT to evaluate and predict hepatic reserve capacity, graft liver function, and the presence of infections.

In this study, we measured Et using the EAA in the peripheral venous blood during living donor liver transplantation (LDLT), to study the clinical significance of the EAA.

## 2. Materials and methods

### 2.1. Subjects

Between April 2010 and February 2011, we performed 21 LDLTs for patients with end-stage liver disease or acute liver failure at the Department of Transplant Surgery, Jichi Medical University, Japan. Of these patients, four with acute renal failure or acute respiratory failure after LDLT underwent apheresis, and were thus excluded from this study. Therefore, this study evaluated 17 patients, eight males and nine females, with a median age of 21 mo (range, 6–229 mo) and a median body weight of 9.7 kg (range, 5.2–49.7 kg). The original disease was biliary atresia (BA) in 12 patients, ornithine transcarbamylase deficiency (OTCD) in three, graft liver failure in one, and primary sclerosing cholangitis in one. The ABO blood type was identical in nine patients, compatible in four, and incompatible in four.

We obtained approval to conduct this study from the Ethics Committees of Jichi Medical University.

### 2.2. Immunosuppression therapy

We used tacrolimus (Tac) and methylprednisolone (MP) as standard postoperative immunosuppression therapy. The target trough level of Tac was 15–20 ng/mL during the first week, 8–12 ng/mL during the first month, 5–8 ng/mL during the first 6 mo, 3–5 ng/mL during the first year, and 2–4 ng/mL thereafter. We administered MP at an initial dose of 20 mL/kg intravenously on the morning of the operation and before graft reperfusion. The MP dose was gradually decreased to 3 mg/kg/d on postoperative Day (POD) 1, 0.5 mg/kg/d on POD 7, and 0.25 mg/kg/d at 1 mo post-LDLT; we discontinued it within 1 y, except in patients for whom immunosuppression could not be maintained with the lower dosage. We used mycophenolate mofetil when more potent immunosuppression was required—for example in ABO-incompatible recipients older than 5 y of age, patients with steroid-resistant acute rejection episodes, and patients with liver dysfunction after cessation of MP therapy.

### 2.3. EAA

We measured the EA in perioperative peripheral venous blood, by EAA at 1 or 2 d before LT, and on PODs 1, 5, 7, 14, and 21 [6,7].

The EAA (Spectral Diagnosis, Inc, Toronto, Ontario, Canada) is a rapid *in vitro* diagnostic test that uses a specific monoclonal antibody to measure the EA in EDTA whole blood specimens. This assay uses the biological response of the neutrophils in a patient's blood to the immunological complex of Et and exogenous antibody as a measure of the Et in these patients. The assay leads to a specific reaction with lipopolysaccharide (LPS) of Gram-negative bacteria or does not cross-react with cell wall constituents of Gram-positive bacteria and other microorganisms. We drew a 1.2-mL sample of whole blood into an Et-free ethylenediaminetetra acetic acid blood collection tube for use in the EAA. We maintained blood samples at room temperature and assayed all samples within 3 h of collection.

The EAA is based on the reaction of Et with a specific anti-Et antibody raised against the lipid A of *Escherichia coli* J5. Complement proteins opsonize the Et–antibody complex. The opsonized immune complex primes neutrophils in the blood to enhance their respiratory burst in response to zymosan. The respiratory burst of the neutrophils yields oxidants that react with luminol in the reaction mixture to emit chemiluminescence. The chemiluminescence can then be detected in a photon counting luminometer (SmartLine TL; Berthold, Huntsville, Alabama).

Basal activity measurement (Tube 1) in the absence of the specific anti-Et antibody measures the nonspecific oxidative burst of the patient's neutrophils. An additional control measurement including the specific anti-Et antibody and an excess of exogenous Et (Tube 3) measures the maximum oxidative burst of the patient's neutrophils. The test measurement (Tube 2) includes the specific antibody to measure the level of EA. All three tubes are incubated at 37°C for 15 min, and then are assayed in triplicate. The EAA level is calculated by normalizing the chemiluminescence in the test sample (Tube 2) against the maximum chemiluminescence (Tube 3), while correcting both measurements for the basal activity chemiluminescence (Tube 1).

An EA level of 0.40 is approximately equivalent to an Et concentration of 25–50 pg/mL, and a level of 0.60 is approximately equivalent to an LPS concentration of 100–200 pg/mL of *E. coli* 055:B5 LPS. For the EA, we considered <0.40 to be a low EA, 0.40–0.60 to be an intermediate EA, and >0.60 to be a high EA.

### 2.4. Limulus amebocyte lysate (LAL) method

The most commonly used diagnostic test, the chromogenic LAL assay, is based on the ability of endotoxins to induce coagulation of the hemolymph in the horseshoe crab, *Limulus polyphemus* [11].

The measurement is conducted using a reaction in which Et and a Limulus reagent derived from horseshoe crab specifically coagulate. A clotting enzyme becomes activated at the final stage of the Limulus cascade and coagulin appears, forming insoluble polymers by further becoming polymerized,

and then forming a gel. Changes in turbidity from this gelation are quantitatively treated.

By carrying out a method of diluting and heating at 70°C for 10 min as a pretreatment method, and using a method of highly sensitive turbidimetric time analysis, we treated the gelation reaction time of a Limulus reagent, which is a substance extracted from horseshoe crab hematocytes, as changes in the amount of transmitted light of the reaction solution. With the reaction time until the amount of transmitted light of the reaction solution decreases by a certain ratio designated as the gelation time, we measured the Et level based on the relationship with Et concentrations.

### 2.5. Statistical analysis

We assessed the differences between groups using the Mann-Whitney U-test and Student's t-test using StatView (SAS Institute, Cary, NC). For all comparisons, differences at $P < 0.05$ were considered statistically significant.

## 3. Results

We measured the EAA 98 times for 17 patients (Table 1). Eight patients had no complications in the postoperative period, but six developed infections and three patients had hyperbilirubinemia or massive ascites (Table 2).

### 3.1. Changes in EA level after LDLT in patients without complications

Patients without complications ($n = 8$) showed a gradual increase in the EA level until 5–7 POD from pre-LT, and decreased gradually thereafter (Fig. 1). The average EA level at pre-LT and 1, 5, 7, 14, and 21 POD was 0.08, 0.16, 0.27, 0.28, 0.22, and 0.17, respectively. We observed a significant difference between pre-LT and 5 or 7 POD ($P = 0.015$ and $P = 0.006$).

### 3.2. Changes in EA level after LDLT in patients with infections

Six patients (35.3%) developed infections; the type of infection was focal peritonitis in two patients, gastroenteritis in two, pneumonia in one, and bacteremia in one. Patients with infections showed a gradual increase in EA level at 5 POD, which decreased gradually until 7 POD, increased gradually again until 14 POD again, and then decreased gradually thereafter (Fig. 2A). The average EA level at pre-LT and 1, 5, 7, 14, and 21 POD was 0.22, 0.24, 0.29, 0.21, 0.45, and 0.30, respectively. We observed a significant difference between 7 and 14 POD ($P = 0.029$).

We compared the EA levels in patients with infections ($n = 6$) with those of patients without complications ($n = 8$), from pre-LT until 21 POD. Patients with infections had significantly higher EA levels compared with those without complications at both pre-LT and 14 POD ($P = 0.038$ and 0.027) (Fig. 2B).

### 3.3. Changes in EA level after LDLT in patients with an EA level of >0.20 before LDLT

Seven patients (41.2%) had an EA level of >0.20 before LDLT. The patients showed a decrease in EA level on 1 POD, which increased gradually until 5 POD, and then decreased gradually thereafter (Fig. 3A). The average EA level at pre-LT ad 1, 5, 7, 14, and 21 POD in these patients was 0.29, 0.20, 0.40, 0.33, 0.37, and 0.31, respectively. We observed no significant differences during the evaluation period.

We compared patients with an EA level of >0.20 before LDLT ($n = 7$) with those without complications ($n = 8$) from pre-LT to 21 POD. Patients with EA levels of >0.20 before LDLT

**Table 1 – Results of endotoxin activity levels determined by the endotoxin activity assay.**

| Case | Original disease | PELD/MELD score | pre-LT | 1 POD | 5 POD | 7 POD | 14 POD | 21 POD |
|---|---|---|---|---|---|---|---|---|
| 1 | OTCD | −9.3 | 0.24 | 0.42 | 0.21 | 0.22 | 0.23 | |
| 2 | BA | 26.9 | 0.22 | 0.29 | 0.63 | 0.45 | 0.47 | |
| 3 | BA | 5.7 | 0.16 | 0.19 | 0.19 | 0.27 | 0.47 | |
| 4 | BA | 11.3 | 0.06 | 0.23 | 0.39 | 0.25 | 0.65 | |
| 5 | BA | 10.7 | 0.01 | 0.18 | 0.46 | 0.17 | 0.23 | |
| 6 | BA | 19.5 | 0.16 | 0.19 | 0.31 | 0.19 | 0.41 | 0.18 |
| 7 | BA | −4.0 | 0.36 | 0.02 | 0.77 | 0.58 | 0.62 | 0.47 |
| 8 | OTCD | −15.8 | 0.29 | 0.13 | 0.19 | 0.37 | 0.16 | 0.18 |
| 9 | BA | 31.3 | 0.08 | 0.17 | 0.22 | 0.23 | 0.29 | 0.06 |
| 10 | BA | 11.8 | 0.03 | 0.05 | 0.10 | 0.24 | 0.02 | 0.05 |
| 11 | PSC | −2.0 | 0.24 | 0.15 | 0.33 | 0.36 | 0.17 | 0.16 |
| 12 | OTCD | −2.3 | 0.02 | 0.02 | 0.53 | 0.33 | 0.26 | 0.48 |
| 13 | BA | −6.2 | 0.26 | 0.26 | 0.25 | 0.06 | 0.38 | 0.25 |
| 14 | BA | −2.2 | 0.06 | 0.38 | 0.28 | 0.38 | 0.24 | 0.03 |
| 15 | BA | −6.4 | 0.13 | 0.08 | 0.31 | 0.21 | 0.11 | 0.24 |
| 16 | BA | −7.9 | 0.05 | 0.29 | 0.09 | 0.28 | 0.44 | 0.15 |
| 17 | graft failure | 7.9 | 0.42 | 0.12 | 0.39 | 0.27 | 0.55 | 0.48 |

OTCD = ornithine transcarbamylase deficiency; PSC = primary sclerosing cholangitis, PELD = pediatric end-stage liver disease; MELD = models for end-stage liver disease.

**Table 2 – Characteristics of patients in the present study.**

| Case | Original disease | Age (mo)/body weight (kg) | PELD/MELD score | ABO incompatibility | GV/SLV (%) | Cold ischemic time (min) | Warm ischemic time (min) | ACR (POD) | CMV-Ag positive (POD) | Others | Discharge |
|---|---|---|---|---|---|---|---|---|---|---|---|
| 1 | OTCD | 10/8.6 | −9.3 | Identical | 95.6 | 102 | 50 | | 31 | Focal peritonitis (5 POD) | 36 POD |
| 2 | BA | 12/5.2 | 26.9 | Identical | 85.7 | 160 | 37 | | | Hyperbilirubinemia | 109 POD |
| 3 | BA | 27/10.7 | 5.7 | Incompatible | 62.2 | 131 | 47 | 20 | | Bacteremia (14 POD) | 37 POD |
| 4 | BA | 14/8.0 | 11.3 | Identical | 82.5 | 118 | 43 | 26 | 35 | Gastroenteritis (14 POD) | 38 POD |
| 5 | BA | 12/8.7 | 10.7 | Incompatible | 80.3 | 176 | 50 | | | | 32 POD |
| 6 | BA | 9/7.8 | 19.5 | Identical | 64.6 | 178 | 39 | 6 | | Gastroenteritis (12 POD) | 29 POD |
| 7 | BA | 124/39.0 | −4.0 | Identical | 36.8 | 405 | 43 | | | Massive ascites | 29 POD |
| 8 | OTCD | 64/20.9 | −15.8 | Compatible | 59.6 | 155 | 49 | | | | 32 POD |
| 9 | BA | 6/7.8 | 31.3 | Compatible | 74.9 | 182 | 48 | | 20 | | 29 POD |
| 10 | BA | 12/7.4 | 11.8 | Identical | 88.0 | 77 | 31 | | | | 27 POD |
| 11 | PSC | 229/47.0 | −2.0 | Compatible | 42.3 | 172 | 70 | | | Hyperbilirubinemia | 17 POD |
| 12 | OTCD | 181/49.7 | −2.3 | Incompatible | 37.4 | 155 | 49 | | 8 | | 26 POD |
| 13 | BA | 153/47.8 | −6.2 | Compatible | 47.0 | 201 | 44 | | | Focal peritonitis (13 POD) | 59 POD |
| 14 | BA | 11/8.1 | −2.2 | Identical | 84.2 | 75 | 39 | | | | 30 POD |
| 15 | BA | 21/9.7 | −6.4 | Identical | 71.9 | 50 | 40 | | | | 38 POD |
| 16 | BA | 193/44.3 | −7.9 | Identical | 33.7 | 130 | 41 | | | | 18 POD |
| 17 | Graft failure | 168/32.8 | 7.9 | Incompatible | 40.2 | 190 | 49 | | 7 | Pneumonia (14 POD) | 64 POD |

GV/SLV = graft volume/standard liver volume; ACR = acute cellular rejection; CMV = cytomegalovirus.
Other abbreviations as in Table 1.